Quaternary Science Reviews 172 (2017) 15–31

Contents lists available at ScienceDirect

Quaternary Science Reviews

journal homepage: www.elsevier.com/locate/quascirev

Rapid and punctuated Late Holocene recession of Siling Co, central Tibet

Xuhua Shi [a, *], Eric Kirby [b], Kevin P. Furlong [c], Kai Meng [d], Ruth Robinson [e], Haijian Lu [f], Erchie Wang [d]

[a] Earth Observatory of Singapore, Nanyang Technological University, 639798, Singapore
[b] College of Earth, Ocean, and Atmospheric Sciences, Oregon State University, Corvallis, OR 97331, USA
[c] Department of Geosciences, The Pennsylvania State University, University Park, PA 16802, USA
[d] Institute of Geology and Geophysics, Chinese Academy of Sciences, Beijing 100029, China
[e] Department of Earth and Environmental Sciences, University of St Andrews, St Andrews KY16 9AL, UK
[f] Institute of Geology, Chinese Academy of Geological Sciences, Beijing 100037, China

ARTICLE INFO

Article history:
Received 4 June 2017
Received in revised form
16 July 2017
Accepted 20 July 2017

Keywords:
Holocene lake level fluctuations
Siling Co shorelines
Tibetan Plateau
Asian monsoon
Holocene abrupt climate change
Hydrologic index

ABSTRACT

Variations in the strength of the Asian monsoon during Holocene time are thought to have been associated with widespread changes in precipitation across much of Tibet. Local records of monsoon strength from cave deposits, ice cores, and lake sediments typically rely on proxy data that relate isotopic variations to changes in precipitation. Lake expansion and contraction in response to changing water balance are likewise inferred from sedimentologic, isotopic and paleobiologic proxies, but relatively few direct records of changes in lake volume from preserved shorelines exist. Here we utilize relict shoreline deposits and associated alluvial fan features around Siling Co, the largest lake in central Tibet, to reconstruct centennial-to-millennial-scale variations in lake area and volume over the Holocene. Mapping and surveying of lacustrine shorelines coupled with optically stimulated luminescence dating of associated deposits indicate protracted occupation of a highstand elevation from >8 ka to 4 ka, followed by rapid recession that was likely punctuated by several stillstands of centennial-scale duration. Calculation of the changes in lake surface area and past hydrologic indices of the Siling Co basin suggests the effective moisture during the early Holocene highstand was approximately three times greater than today. In contrast to other lakes in central and western Tibet, our results suggest that Siling Co did not begin to recede synchronously with decreasing solar insolation at ca. 9–8 ka. Rather, initial recession of Siling Co appears to correspond to a time period of enhanced aridity and weakened monsoon in both Africa and Asia at ca. 4.2 ka. Our results add to a growing body of literature that suggest a period of relatively severe aridity on the Tibetan Plateau at this time. We suggest that subsequent punctuated recession of Siling Co was punctuated by similar periods of abrupt climate change during the Late Holocene.

© 2017 The Authors. Published by Elsevier Ltd. This is an open access article under the CC BY-NC-ND license (http://creativecommons.org/licenses/by-nc-nd/4.0/).

1. Introduction

Hundreds of saline lakes decorate the southern Tibetan Plateau (Fig. 1) (Zhang et al., 2014), where modern precipitation is largely driven by the Asian monsoons (Gasse et al., 1991; Hudson et al., 2015; Tian et al., 2001a). These lakes provide important archives of past changes in monsoon-related precipitation (Gu et al., 1993; Hudson and Quade, 2013). Variations in monsoon strength are often inferred from sedimentologic proxies (e.g., Gasse et al., 1991; Mischke and Zhang, 2010), isotopic composition of lacustrine sediments (e.g., $\delta^{18}O$, $\delta^{13}C$, δD_{wax}, Mg/Ca) (e.g., Bird et al., 2014; Gasse et al., 1991, 1996; Morrill et al., 2006; Mügler et al., 2010), and palynologic and paleontologic records (e.g., Herzschuh et al., 2006; Li et al., 2011; Morrill et al., 2006; Van Campo et al., 1996; Zhu et al., 2010, 2015). Similarly, shifts in the stable isotopic (e.g., $\delta^{18}O$) composition of speleothem carbonate (e.g., Fleitmann et al., 2003; Wang et al., 2005), ice cores (e.g., Thompson et al., 2000), and peat bogs (Hong et al., 2003) all suggest that monsoonal precipitation over the Asian continent reached a maximum in the early Holocene, coincident with a maximum in solar insolation (Berger, 1978). Although these proxies provide relatively precise temporal

* Corresponding author.
E-mail address: xshi@ntu.edu.sg (X. Shi).

http://dx.doi.org/10.1016/j.quascirev.2017.07.017
0277-3791/© 2017 The Authors. Published by Elsevier Ltd. This is an open access article under the CC BY-NC-ND license (http://creativecommons.org/licenses/by-nc-nd/4.0/).

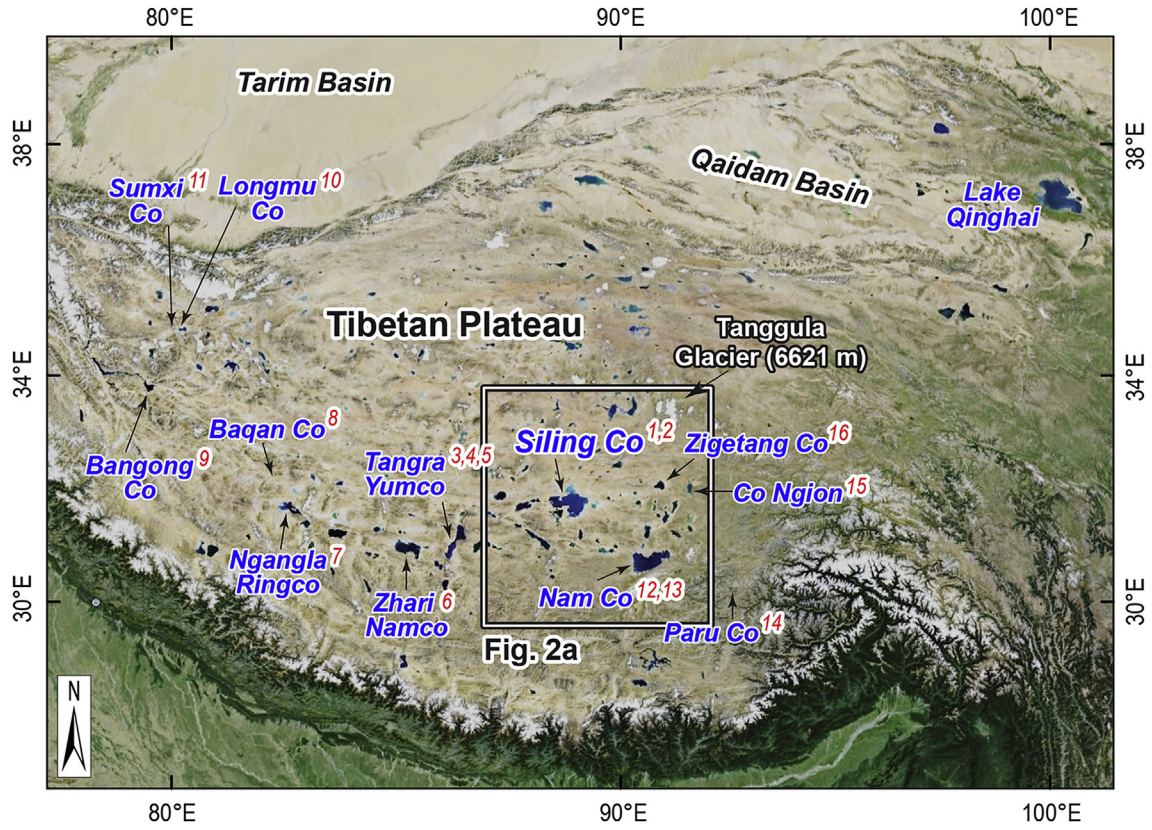

Fig. 1. Google Earth satellite image showing the locations of major lakes in closed basins in the Tibetan Plateau. The red numbers labeled next to the lake names refer to previous studies of Tibetan lakes mentioned in the text: 1-Gu et al., 1993; 2-Kashiwaya et al., 1995; 3-Rades et al., 2013; 4-Rades et al., 2015; 5-Ahlborn et al., 2016; 6-Chen et al., 2013; 7-Hudson et al., 2015; 8-Huth et al., 2015; 9-Gasse et al., 1996; 10-Liu et al., 2016; 11-Kong et al., 2007; 12-Mügler et al., 2010; 13-Li et al., 2011; 14-Bird et al., 2014; 15-Shen et al., 2008; 16-Herzschuh et al., 2006. (For interpretation of the references to colour in this figure legend, the reader is referred to the web version of this article.)

resolution of variations in monsoon strength, they place only loose bounds on the magnitude of concomitant variations in precipitation. For example, variations in the amplitude of $\delta^{18}O$ may reflect changes in both moisture sources and/or transport pathways (Cai et al., 2012; Dayem et al., 2010; Tian et al., 2001b), as well as changes in the magnitude of precipitation.

Flights of well-preserved paleoshorelines around lakes in Tibet, however, provide a means of estimating changes in lake volume through time (e.g., Benson et al., 1990; Reheis et al., 2014). Because the storage of water in a closed lake basin reflects the balance between evaporation and water influx, as both runoff and direct precipitation (Benson and Paillet, 1989), reconstruction of lake size and volume from studies of paleoshorelines serves as an important complement to stratigraphic records from lake cores. A number of recent studies in western Tibet reconstruct lake history from paleoshoreline positions (Fig. 1) (Ahlborn et al., 2016; Chen et al., 2013; Hudson et al., 2015; Huth et al., 2015; Kong et al., 2007; Liu et al., 2016; Rades et al., 2013, 2015). These studies suggest that most Tibetan lakes reached their maximum extents during the latest Pleistocene or early Holocene and began to recede by ca. 8–9 ka. Although this recession appears to be relatively continuous throughout the Holocene in many records (e.g., Ahlborn et al., 2016; Chen et al., 2013; Rades et al., 2015), a few lakes exhibit punctuated recession, marked by periods of apparent lake level stability (Hudson et al., 2015; Huth et al., 2015; Liu et al., 2016). The significance of this variation in the rate of lake recession is not well understood, in part due to limited studies of lake level history in central and eastern Tibet (Fig. 1).

Here we develop a relatively precise chronology of Holocene lake level change from recessional shorelines and associated alluvial fans around Siling Co ('co' means lake in Tibetan) (Figs. 1 and 2), the largest lake in central Tibet. We mapped and surveyed recessional shoreline deposits and geomorphic features along and below the "Lingtong highstand", a group of shoreline features that developed during the maximum extent of Siling Co in the early Holocene (Shi et al., 2015). We utilize optically stimulated luminescence (OSL) dating (e.g., Aitken, 1998) to characterize the duration of the Holocene highstand and to place bounds on history of lake recession. Geomorphic and stratigraphic associations of groups of paleoshorelines and alluvial fan deposits reveal a punctuated lake level history for Siling Co during the Late Holocene. The positions of these deposits allow reconstruction of lake surface area and volume change through time. We use a simple calculation of hydrologic indices to semi-quantitatively assess differences in effective moisture over the Siling Co basin. Our results, when compared to similar studies of other lakes in western Tibet (e.g., Hudson et al., 2015; Huth et al., 2015; Liu et al., 2016), provide evidence for centennial-length abrupt changes in the relative aridity on the Tibetan Plateau during the Holocene.

2. Study area

The Siling Co basin in central Tibet has a total drainage area of ~5.72×10^{10} m^2 and contains several large lakes that are presently connected through rivers (Fig. 2a). The largest of these is Siling Co, with a lake surface area of ~2.32×10^9 m^2 in 2010 (Meng et al., 2012a). Presently, influx to Siling Co is dominantly from precipitation associated with the Southwest Indian monsoon (Gu et al.,

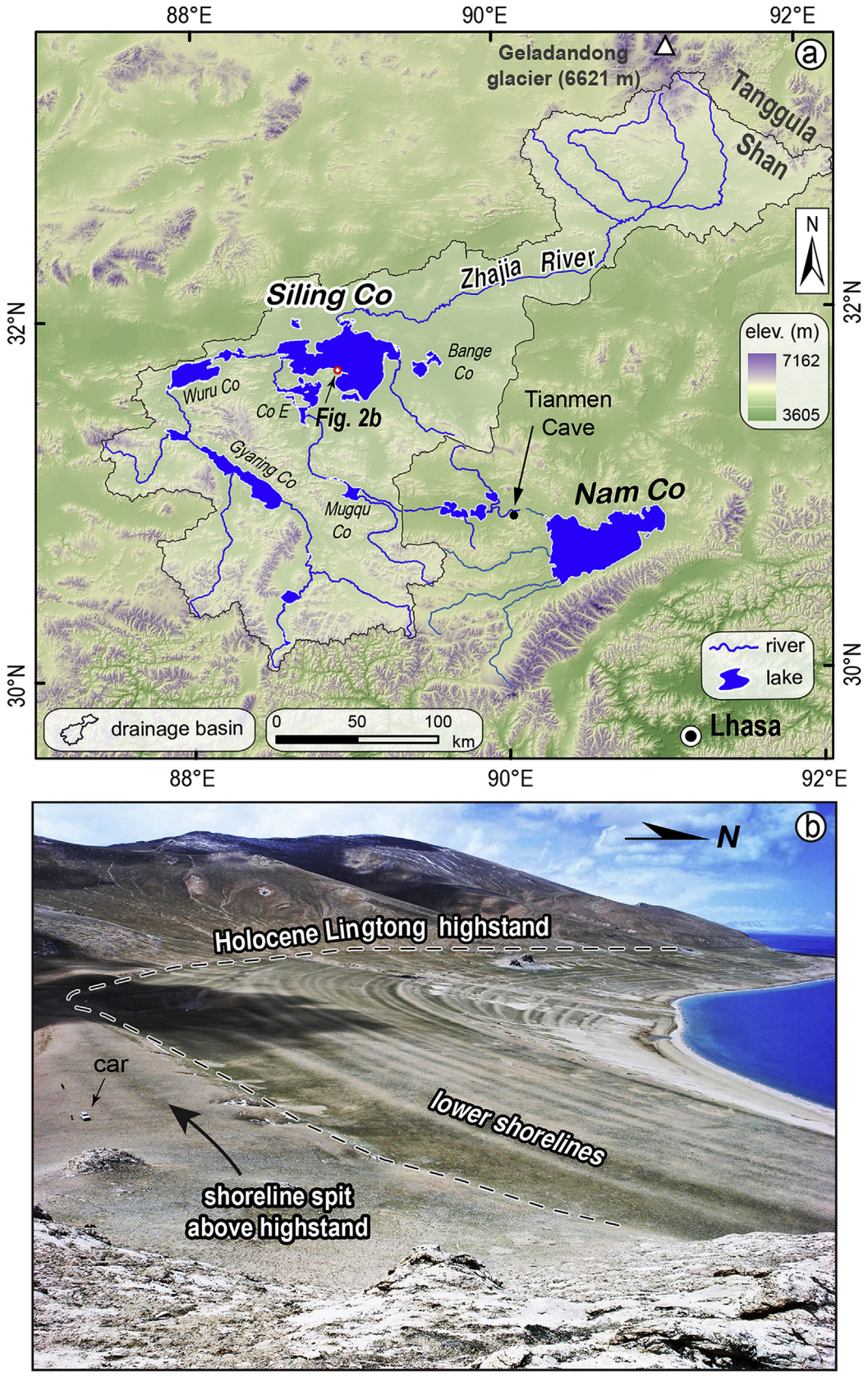

Fig. 2. Present-day hydrologic system of the Siling Co basin. (a) The map showing the lake distribution within the drainage basin and major rivers flowing to Siling Co and Nam Co. (b) Photograph of shoreline groups developed on the NE promontory of the central peninsula of Siling Co.

1993; Tong et al., 2016; Zhou et al., 2015) as well as the Zhajia River (Fig. 2a), which carries meltwater sourced from the distant Geladandong glacier in the Tanggula Shan (Meng et al., 2012a; Tong et al., 2016). Mean annual rates of precipitation over the lake surface and the land area within the basin are ~0.3–0.5 m/yr; mean annual rates of the evapotranspiration over the lake surface and the land area are ~1.0–1.2 m/yr and ~0.4 m/yr, respectively (Tong et al., 2016; Zhou et al., 2015). The total discharge of surface water to the lake, averaged over 2003–2012, is ~0.28 $\times$ 10^9 m^3/yr (Zhou et al., 2015), or ~0.12 m/yr based on the lake surface area of Siling Co in 2010 (Meng et al., 2012a).

Although historical records suggest that lake levels remained fairly stable from the 1970s through the 1990s (Doin et al., 2015; Meng et al., 2012a; Tong et al., 2016), Siling Co began rising in 1998–1999. Since then, the lake level has risen by ~12 m from ~4530 m in elevation in 1976–~4542 m in 2010 (Doin et al., 2015; Meng et al., 2012a; Tong et al., 2016) and has apparently stabilized since then (Tong et al., 2016). Although some studies have argued that the rapid lake rise may be primarily driven by recent glacier meltwater from the Tanggula Shan (Fig. 2) (e.g., Meng et al., 2012a; Zhang et al., 2011), more recent analyses of water balance suggest that variations in precipitation and runoff may be the primary drivers of historic changes in lake levels (e.g., Tong et al., 2016; Zhou et al., 2015).

Paleoshorelines around Siling Co indicate that there were significantly higher past lake levels; the highest shorelines reach >60–110 m above the 1976 lake level (Meng et al., 2012b; Shi et al., 2015) suggesting a lake nearly four times larger in areal extent than today (Shi et al., 2015). Recent studies show that the geomorphic characteristics and positions of these shorelines reflect their age and position relative to a prominent highstand shoreline complex at ~4594 m elevation, the Lingtong highstand (Shi et al., 2015). Beach deposits along this shoreline complex were dated to between 8 and 4 ka by optically stimulated luminescence (Shi et al., 2015), similar in age to an independently dated highstand shoreline around Gyaring Co, one of the upstream basins southwest of Siling Co (Fig. 2a) (Shi et al., 2014). Shorelines above ~4594 m in the Siling Co basin are significantly degraded relative to this highstand and exhibit polygonal fractures and patterned ground characteristic of extensive permafrost activity, suggesting that they are significantly older than the Holocene highstand. Recent dating of several of these higher beach ridges suggests they were deposited between ~110 and 190 ka (Shi et al., 2017). Shorelines below the ~4594 m level, in contrast, are geomorphically fresh, with well-preserved depositional morphology, and exhibit no patterned ground (Fig. 2b); these observations suggest that lower shorelines reflect recessional features developed during Holocene lake recession (Shi et al., 2015). Here, we provide new age constraints on these recessional shorelines and associated alluvial deposits, in an effort to evaluate the pace and tempo of lake recession.

3. Geomorphology and stratigraphy of shoreline deposits

We mapped a total of 1150 individual shoreline features below the Lingtong highstand around Siling Co and its adjacent lakes (Fig. 3), using high-resolution Google Earth satellite imagery (nominal resolution of 0.5 m) and field investigations. These shorelines, in general, cluster in space, and can be classified into six groups. Each group is composed of several laterally continuous beach ridges and associated back-ridge depressions (Figs. 4 and 5). These prominent shorelines are often marked by spits and tombolos, and they grade laterally into wave-cut cliffs in rocky promontories. The continuity and spacing of different shoreline clusters vary with local topography, substrate, and angle of wave attack. For instance, in regions of gentle topography (Fig. 3), the shorelines are more continuous and exhibit wider spacing between clusters. Despite these minor variations, the elevations of primary shoreline groups remain relatively consistent around the entire Siling Co basin. Our field surveys of these shoreline features using differential global positioning system (dGPS) techniques show that groups of shorelines are found approximately at 4545–4555 m (Group 1), 4559–4564 m (Group 2), 4568–4571 m (Group 3), 4573–4576 m (Group 4), 4578–4583 m (Group 5) and 4588–4594 m (Group 6) (Figs. 4 and 5).

We focused our field work and sampling of shoreline features along a well-exposed and accessible embayment along the eastern side of the central peninsula of Siling Co (Fig. 5). Recessional shorelines below the Lingtong highstand level at this location are separated into the six primary groups (G1-G6) described above (Fig. 5). In particular, shorelines at this site are dissected by an ephemeral channel (referred to as the 'Tashi stream'), allowing relatively clear cross-sectional exposures of many of the shoreline and associated alluvial fan deposits (Fig. 5c). In plan view, each shoreline cluster is characterized by one or two sets of prominent beach ridges (Fig. 5c) with convex-upward facing crests (Figs. 5b and 6b). Exposures of the stratigraphy associated with these shoreline deposits show sub-rounded, well-sorted sand and gravel (Figs. 6 and 7) with moderate to steeply dipping cross-bedding that reflect deposition in a nearshore and beach environment.

Alluvial fans (*I* to *VI* in Fig. 5c) are present upslope of each of the prominent shoreline ridges, along the Tashi Stream. These fans are separated from one another by prominent shorelines of each shoreline group, and all have been incised by the ephemeral channel. Alluvial fan deposits consist of relatively unconsolidated sand and fine gravel (Fig. 6); bedding is generally massive but sometimes includes moderate to well-sorted lenses of sand and gravel. Sand layers incorporate clasts of well-rounded beach gravels, some of which are enveloped in a matrix of fine sands, silt and mud (Fig. 6). Observations of the surfaces of beach ridges in pit excavations suggest that the lower shorelines have thin (0–10 cm) eolian silt layers atop open framework beach gravels. This observation is consistent with the preservation of alluvial features such as bar-and-swale topography on fan deposits associated with the lower shorelines (Fig. 6). We infer that both shorelines and alluvial fans become progressively younger toward the modern lake level, and that alluvial fans reflect deposition during periods of relative lake stability, when the lake formed a stable base level to the channel. This is exemplified by the association of the most recent alluvial fan (I) near the current lake level (Fig. 5c). It appears that incision along the Tashi stream occurred progressively, as local base level fell, and the depositional surfaces of both shorelines and alluvial fans were abandoned.

To reconstruct lake levels from these geomorphic features, we surveyed shorelines and associated alluvial fan features in this region using dGPS; original data and methodology can be found in (Meng et al., 2012a, 2012b). Although most survey results allowed for better than decimeter precision in the relative vertical position of the site location and modern lake level (Meng et al., 2012a), uncertainty in paleo-water depth is estimated to be ~50 cm (see discussion in Shi et al. (2015)). The vertical elevation ranges of each of the six groups of shoreline clusters (G1-G6, Fig. 5a and c) are ~$\leq$5 m (Fig. 5b).

4. Methods: age of shoreline deposits

Samples for optically stimulated luminescence (OSL) dating were collected from stream-cut natural exposures of stratigraphy in the channel wall, or from hand-excavated pits (>0.5–1.8 m deep) into shoreline deposits. All OSL samples were carefully collected from sand layers or lenses that were interbedded with the upper

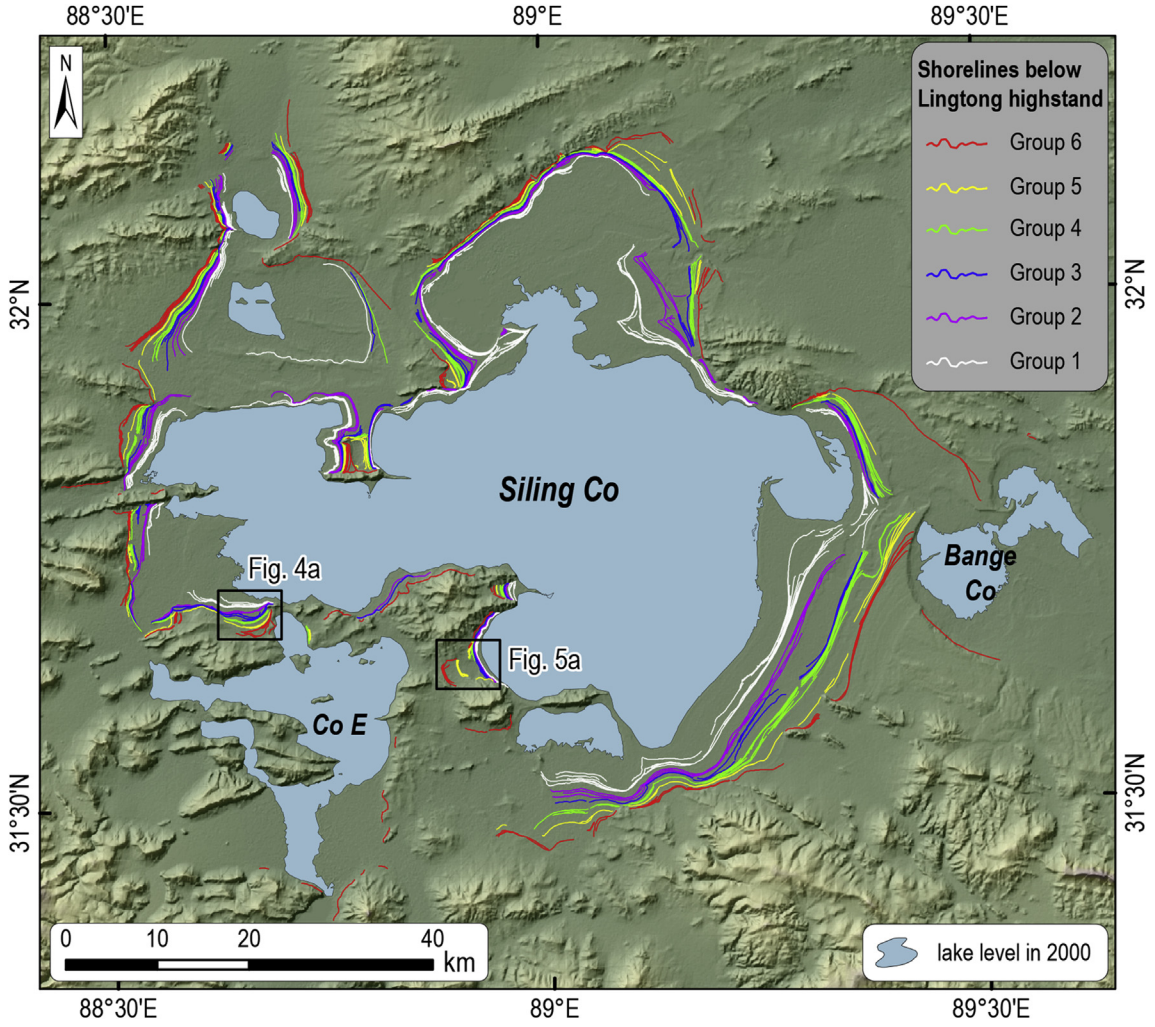

Fig. 3. The map showing that the shorelines around Siling Co are characterized by six clusters at different elevation ranges.

beach facies (Fig. 7) or with alluvial fan deposits ponded upstream of shoreline berms (Fig. 6). Sampling locations were selected to ensure that the age of deposition is a reasonable measure of the timing of shoreline occupation or fan deposition. Although dune complexes are not evident in the region, we avoided sampling sands deposited on top of beach gravels that might have been deposited by eolian processes. Before collecting the sand samples, several centimeters of the exposure surface were removed to eliminate possible uncertainty in history of light exposure (Aitken, 1998). We sampled fine-to medium-sized sand using PVC or steel tubes, 3 cm or 5 cm in diameter, depending on the consolidation and thickness of the sand layers. These tubes were then wrapped with heavy duty black duct tape to avoid light penetration and preserve water content.

We prepared the samples using standard OSL procedures at the University of St. Andrews, Scotland. Sample material was desiccated at 50 °C to enable calculation of water content, and then sieved to extract the quartz fraction of 180–212-μm grain size. We analyzed the samples using the single aliquot regenerative dose (SAR) protocol (Murray and Wintle, 2000). We determined the equivalent dose (D_e) by measuring the luminescence response, following stimulation of the natural luminescence (L_n) and numerous different regenerative doses (L_x). We then normalized the L_n and L_x measurements by the luminescence response (T_x) to a constant test dose (TD). The L_x/T_x ratio is used to compensate for sensitivity changes of the quartz throughout analysis and obtain a range of values which bracket L_n/T_x, allowing D_e interpolation with minimal associated errors (Banerjee et al., 2000). We calculated the environmental dose rates (D_r) for each sample from unsieved parts of original samples. We directly measured concentrations of U, Th, K and Rb using solution ICP-MS (Thermo X-Series), a cosmic-dose component after Prescott and Hutton (1994) and an internal alpha dose rate of 5% from the decay of U and Th after Sutton and Zimmerman (1978). We ignored external α-dose rates because the alpha-irradiated portion of quartz grains was removed by etching. We used the conversion factors of Adamiec and Aitken (1998) and beta-particle attenuation factors after Mejdahl (1979) and Readhead (2002a, 2002b). We calculated sample water content following desiccation at 50 °C, and assume an uncertainty of 5%. Details about laboratory sample processing and analysis can be found in the Supplemental Material of our previous paper (Shi et al., 2015), and Table S2 contains the dosimetry data of OSL samples from the recessional shorelines.

For the OSL age calculation, we analyzed the OSL data (using an Excel spreadsheet) to calculate over-dispersion and statistical parameters and model the appropriate burial age (Db). We then adopted the age model selection criteria of Arnold and Roberts (2009). Most of our samples show large over-dispersion values, i.e. broad D_e distributions (Fig. 8), which describe the spread in the data not accounted for analytical uncertainties (Galbraith and

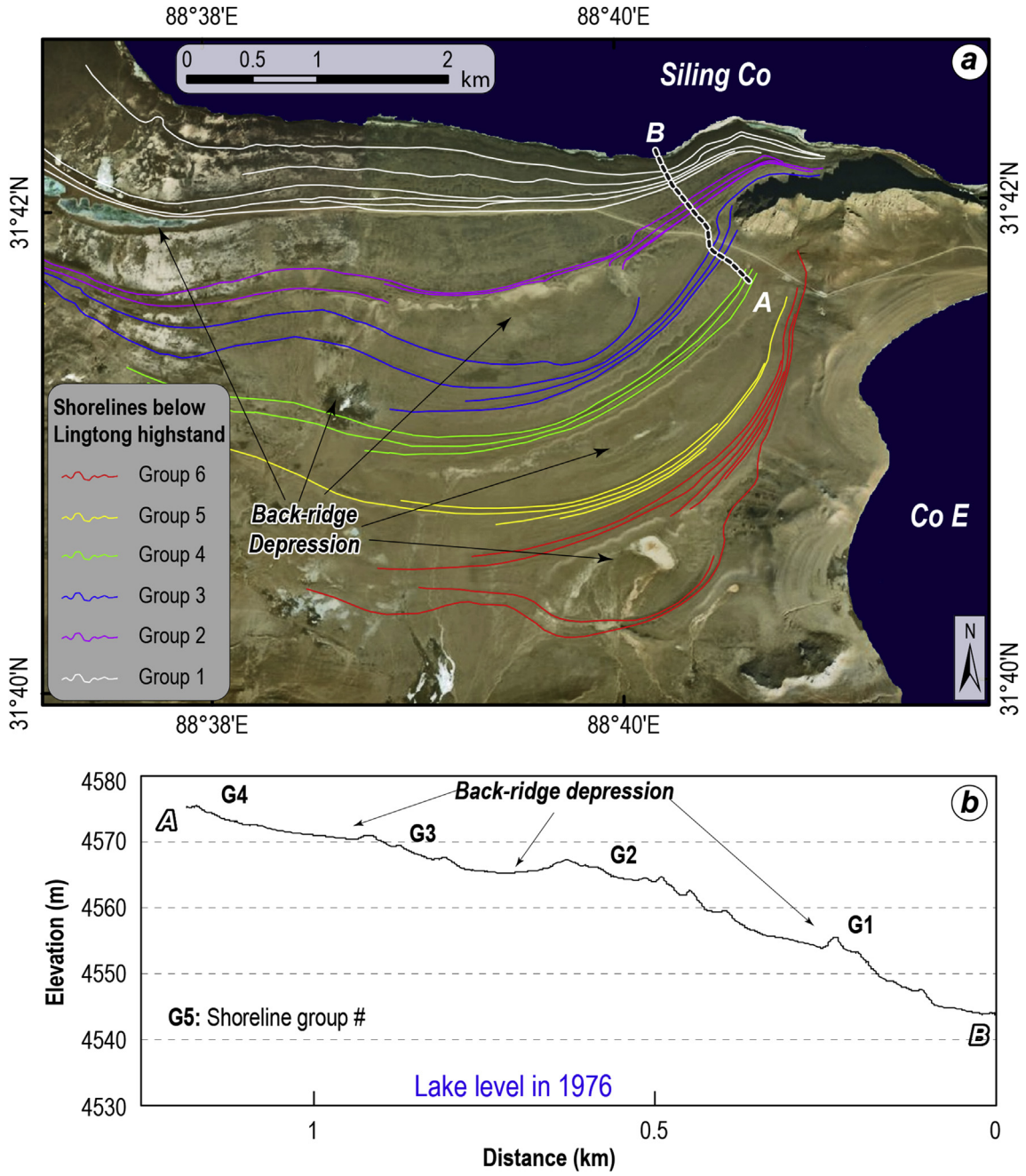

Fig. 4. The geomorphology and topography of clustered shoreline features in southwestern Siling Co (see location in Fig. 3). (a) Clustered shoreline features similar to those in the central peninsula, atop the Google Earth imagery. (b) The topographic profile of the lower parts of the shoreline features (see profile location in Fig. 4a).

Roberts, 2012). Samples with over-dispersion, greater than 20%, are assumed to reflect heterogeneous bleaching before deposition. The data are distributed and in multi-grain analyses, the clear differentiation of separate populations is not straight forward (Arnold and Roberts, 2009). In the calculation, we used all aliquots in the calculation of D_e and did not exclude any data from the analyses. Because most samples show broad D_e over-dispersion, we modeled these samples using the three-component minimum age model (MAM-3, Galbraith et al., 1999) and the RStudio Luminescence package (Kreutzer et al., 2012). In cases where the MAM-3 model fails to capture the lowest population of D_e values, and thus fails to calculate an age, however, we adopted the central age model (CAM) (Galbraith and Green, 1990) to calculate the OSL ages (e.g., O7 in Fig. 8).

5. Late Holocene centennial-millennial-scale lake level history of Siling Co

We collected seven new samples from three shoreline groups (G5, G2 and G1) below the Lingtong highstand shoreline complex (G6 complex in Fig. 5). Previously, we obtained an age from the highstand of 7.8 ± 0.4 ka (Shi et al., 2015); some aliquots from this sample suggest a second, younger component of the age distribution of 3.9 ± 0.3 ka. This younger age is consistent with 8 additional samples that suggest occupation of the Lintong highstand (G6) until ca. 4 ka (Shi et al., 2015). Three of our new samples were taken from

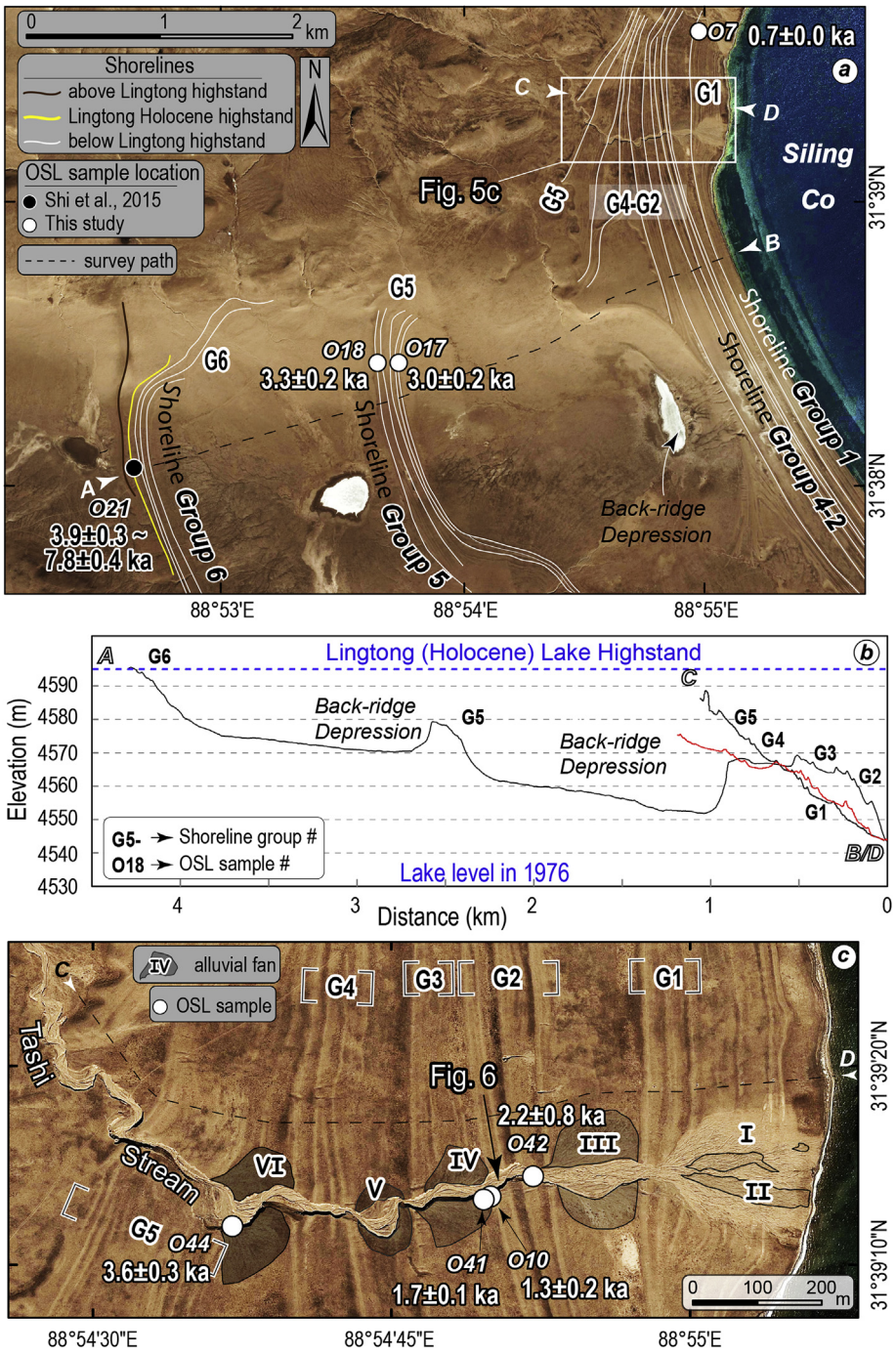

Fig. 5. Topographic and geomorphic features of shorelines and alluvial fans developed on the central peninsula of Siling Co. (a) GeoEye image (nominal resolution of 0.5 m) showing the shoreline features (white lines) and OSL sample locations. Ages are shown with 2-sigma uncertainties. (b) Topographic profiles of shoreline elevations in the central peninsula (black lines, see locations in Fig. 5a and c) and southwest of Siling Co (red line, see profile location in Fig. 4a). (c) Close-up of GeoEye image showing the shorelines and alluvial fans developed along the Tashi Stream (see location in Fig. 5a). (For interpretation of the references to colour in this figure legend, the reader is referred to the web version of this article.)

beach ridges associated with the G5 complex, and place a direct lower bound on the age of initial recession from the highstand (Fig. 9). Moreover, the range of ages of these samples provides an estimate of the duration of the stillstands associated with the G5 complex. Two additional samples were collected from beach ridges in the lower G2 shoreline group were collected from beach ridges, while a third sample (O10) was collected from a sand layer in the alluvial fan that onlaps the G2 shoreline (Fig. 6). This alluvial sample (O10) is expected to be younger than the beach sample (O41), and the age difference may provide an estimate of the lag time between shoreline occupation and alluvial fan deposition. Finally, we collected a single sample from the alluvial fan developed atop a G1 shoreline foreset; this sample provides a lower bound on the timing of development of the G1 shoreline complex. Unfortunately, we were unable to obtain appropriate sample material for dating from the beach deposits in G4, G3 and G1 shorelines.

Samples from the G5 shoreline groups yield reasonably well-clustered OSL ages (Figs. 8 and 9) of 3.6 ± 0.3 ka (sample O44),

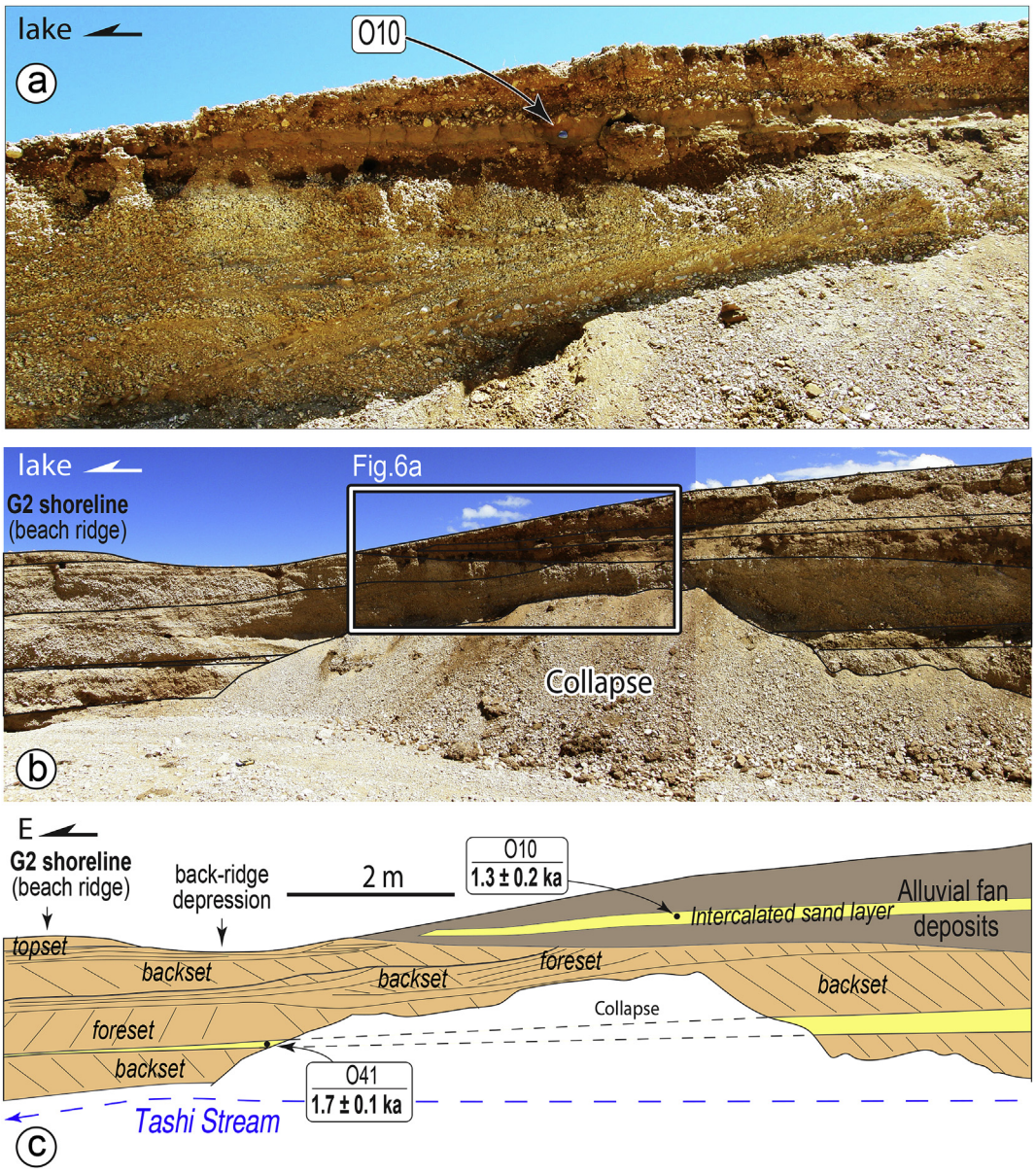

Fig. 6. Field photos (a–b) and sketch (c) of stratigraphic relations above the G2 shorelines along the Tashi Stream. At this location, samples O41 and O10 were collected from the beach deposits and alluvial sand layer, respectively. A close view of the sample O10 site is shown in panel (a).

3.3 ± 0.2 ka (sample O18) and 3.0 ± 0.2 ka (sample O17) (Table 1). In combination with the youngest age from the highstand shoreline (~3.9 ± 0.3 ka; sample O21 of Shi et al. (2015), location in Fig. 5a), these results place rather tight constraints on the initial timing of recession, suggesting that it likely occurred between 4.2 and 3.9 ka, within uncertainties (Fig. 9b). Moreover, the minimal variation in elevation (4574–4578 m) of G5 shorelines suggest that the lake maintained a relatively stable level during the time period following initial recession, between ~3.9 ka and 2.8 ka.

Sample ages from G2 shorelines also yield reasonably similar ages of 2.2 ± 0.8 ka (sample O42) and 1.7 ± 0.1 ka (sample O41) (Fig. 9b; Table 1). A third sample collected from alluvial fan deposits (sample O10; Table 1) above the shoreline (and above sample O41) yields an age of 1.3 ± 0.2 ka, suggesting the lake level was below this elevation by this time. Together, these results suggest that the lake was relatively stable around 4562 m for ~1 ka (between ~2.2–1.3 ka) or possibly longer considering the age uncertainties. These results also suggest that recession from G5 shorelines occurred at ~3.2–3.0 ka (Fig. 9b). Finally, the age difference of ~400 ± 300 years between samples O41 (beach) and O10 (alluvial fan) reinforces our inference that the development of alluvial fans upstream of beach ridges reflects a lake stillstand that appears to have a centennial-scale duration. This is also consistent with the age of the alluvial sample taken from sits atop G1 shorelines (sample O7), ~0.7 ka (Figs. 5a and 9b). This result places a bound that this lowest group of shorelines was established by ~0.7 ka.

Our results demonstrate that Siling Co underwent a rapid but stepwise recession by ~64 m, since ~4 ka. Following a relatively stable highstand elevation from 6 to 8 ka to ~4 ka (Shi et al., 2015), the lake dropped at an average rate of 16 m per 1000 years (Fig. 9b). Notably, that recession was punctuated by periods of relatively stable lake levels. The OSL chronology confirms our geomorphic interpretation that alluvial fan deposition reflects short-lived (<ca. 1 ka) periods of lake level stability, as exemplified by ages of G5 and G2 shorelines. A shorter lake stillstand may be allowable given the single age (O7) from the G1 shorelines. However, the lack of

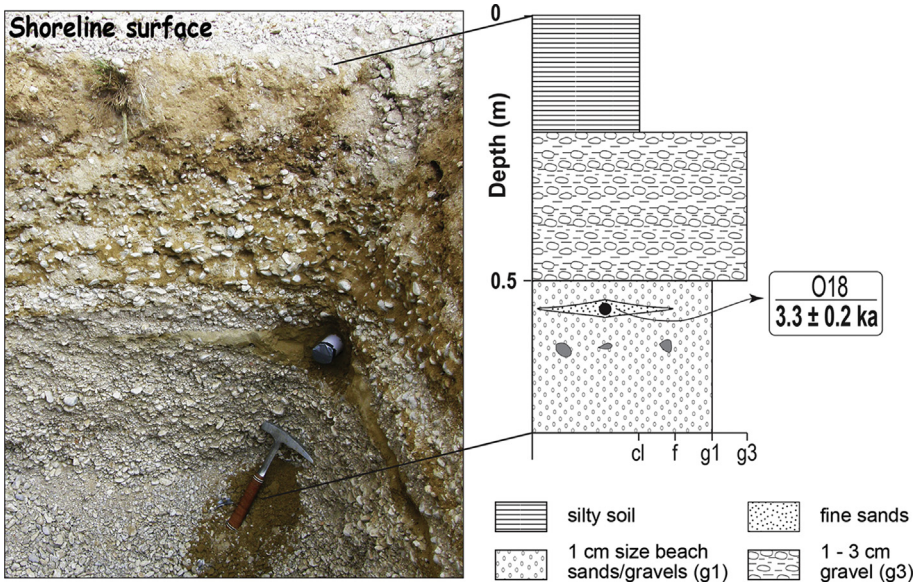

Fig. 7. Field photograph showing a soil pit dug into a beach ridge shoreline of the G2 group. Deposits are characterized by well-sorted, rounded gravel and cobble clasts with interbedded sand lenses. OSL sample (O18, see location in Fig. 5a) show in position.

multiple samples from this shoreline group at this site makes this interpretation somewhat tentative (Fig. 9b). The intervening times between the lake stillstands appear to reflect periods of rapid lake recession on the order of ~10–20 m in elevation. These recessions appear to have begun at ~4 ka, ~3 ka, ~1.3 ka and ~0.7 ka. Although the chronology is not sufficient to precisely resolve the duration of these recessions, it appears from the range of our data that they occur within intervals as short as ~100–500 years (Fig. 9b). The spatial proximity of G4 and G3 shoreline clusters and associated alluvial fans *VI-IV* (Fig. 5b and c) may suggest even shorter stillstands between ca. 3 and ca. 1 ka (Fig. 9b).

Our results provide insights into the lake level history of Siling Co since the Late Holocene, on centennial and millennial scales. It is important to note that we are unable to resolve decadal scale variations that are commonly seen in paleoclimatic studies based on radiocarbon dating of lacustrine core sediments (e.g., Bird et al., 2014) or speleothems (e.g., Wang et al., 2005). Such variations in lake levels almost certainly occurred within the time period of our record, as exemplified by the lake rise of ~10 m during 1998–2010 (Doin et al., 2015; Meng et al., 2012a; Tong et al., 2016). However, the observation that alluvial fans are ponded against the upstream faces of beach ridges requires that the lake surface remain at or near the elevation of the shoreline clusters for a sufficient amount of time to accumulate such alluvial deposits. Our chronology suggests that these clusters represent hundreds to perhaps thousands of years. In addition, the Lingtong highstand shoreline complex has been deflected from the horizontal by up to 2–4 m (Shi et al., 2015), requiring the lake to have been stable for sufficient time for the crust to flex downward under the water load (Shi et al., 2015). Decadal-scale high frequency lake fluctuations very likely erode and rework previously developed shoreline features. For example, historic satellite images reveal that the lake shorelines of Siling Co developed before its lake rise in 1998 were reworked and destroyed during 2009–2012 (also ref. Meng et al., 2012a).

6. Past changes in the hydrological index of Siling Co

The hydrologic index (*HI*) is an estimate of the effective moisture conditions under equilibrium, which is the ratio of lake surface area to the land tributary area such that the water in and out of the lake is equal (Benson and Paillet, 1989; Hudson and Quade, 2013; Mifflin and Wheat, 1979), shown as the formula below.

$$HI = \frac{A_w}{A_l} = \frac{A_w}{(A_b - A_w)}$$

where A_b, A_l and A_w are the area of the entire drainage basin, the land and the lake surface, respectively. Importantly, for a drainage basin that contains multiple lakes of variable size and geometry, calculation of the *HI* index requires including the surface areas of all lakes within that basin (Benson et al., 1990; Benson and Paillet, 1989). In this study, we determine the *HI* index at the time of the Lingtong highstand to evaluate the effective moisture over the lake basin to provide some insights into future research on changes in past water balance of this region. Examples of such application can be found in previous studies of lakes in western Tibet (Hudson and Quade, 2013; Hudson et al., 2015; Huth et al., 2015).

We reconstructed the lake surface area of Siling Co at the time of each stillstand (Fig. 9c) to calculate *HI*. The lake surface area was calculated from the area of polygons defined at specific shoreline elevations, based on the 90-m-resolution shuttle radar topography mission (SRTM) data (Farr et al., 2007). We use Siling Co and Gyaring Co (Shi et al., 2014) to calculate the total lake surface area in the basin, as the other lakes in the basin are very small in size (Fig. 2a) and do not contribute significantly to the calculation (Fig. 9c). Our results indicate that the area of Siling Co shrank at an overall rate of ~1.42 × 10^6 m^2 per 1000 years since ~4 ka, from ~7.351 × 10^9 m^2 at 4 ka to ~1.667 × 10^9 m^2 in 1976 (Fig. 9a and c, Table S3). Likewise, the area of Gyaring Co reduced from ~6.74 × 10^8 m^2 to ~2.76 × 10^8 m^2. The drainage area of the Siling Co basin is ~5.72 × 10^{10} m^2, implying a *HI* of ~0.15 at 4 ka and modern *HI* of ~0.05 in 1976 (Table S3). This simple analysis suggests a climate state at ~4 ka that was associated with an *HI* approximately three times greater than today. This index is not a direct measure of changes in precipitation, but rather represents a combination of enhanced precipitation and reduced evapotranspiration during this time.

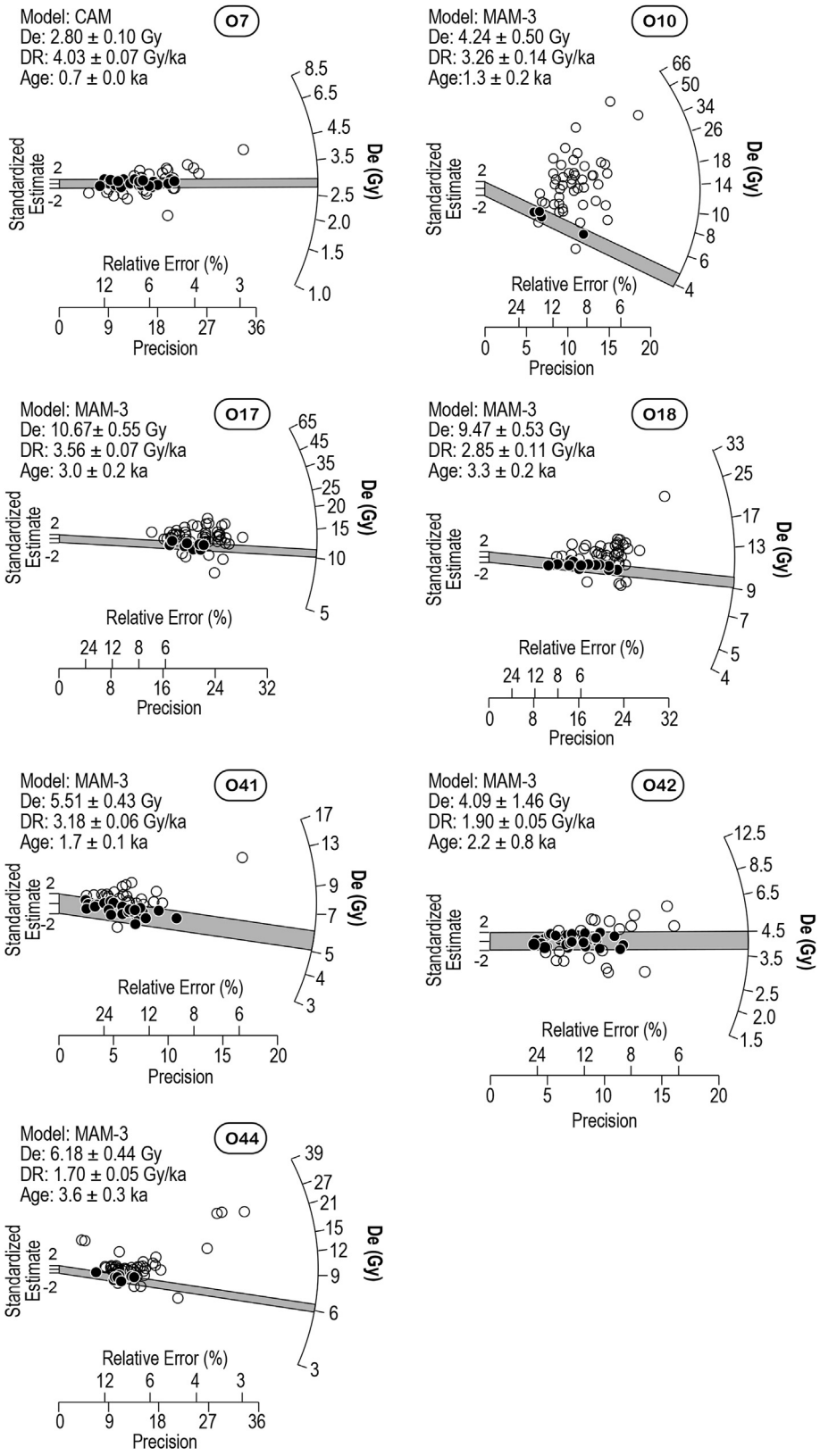

Fig. 8. Radial plots showing distributions of equivalent dose (D_e) and uncertainties of OSL samples from this study. Note that the open circles in the radial plots fall outside of the 2-standard estimate range and are therefore differentiated from the data points that fall within that range, but they are included in the analysis.

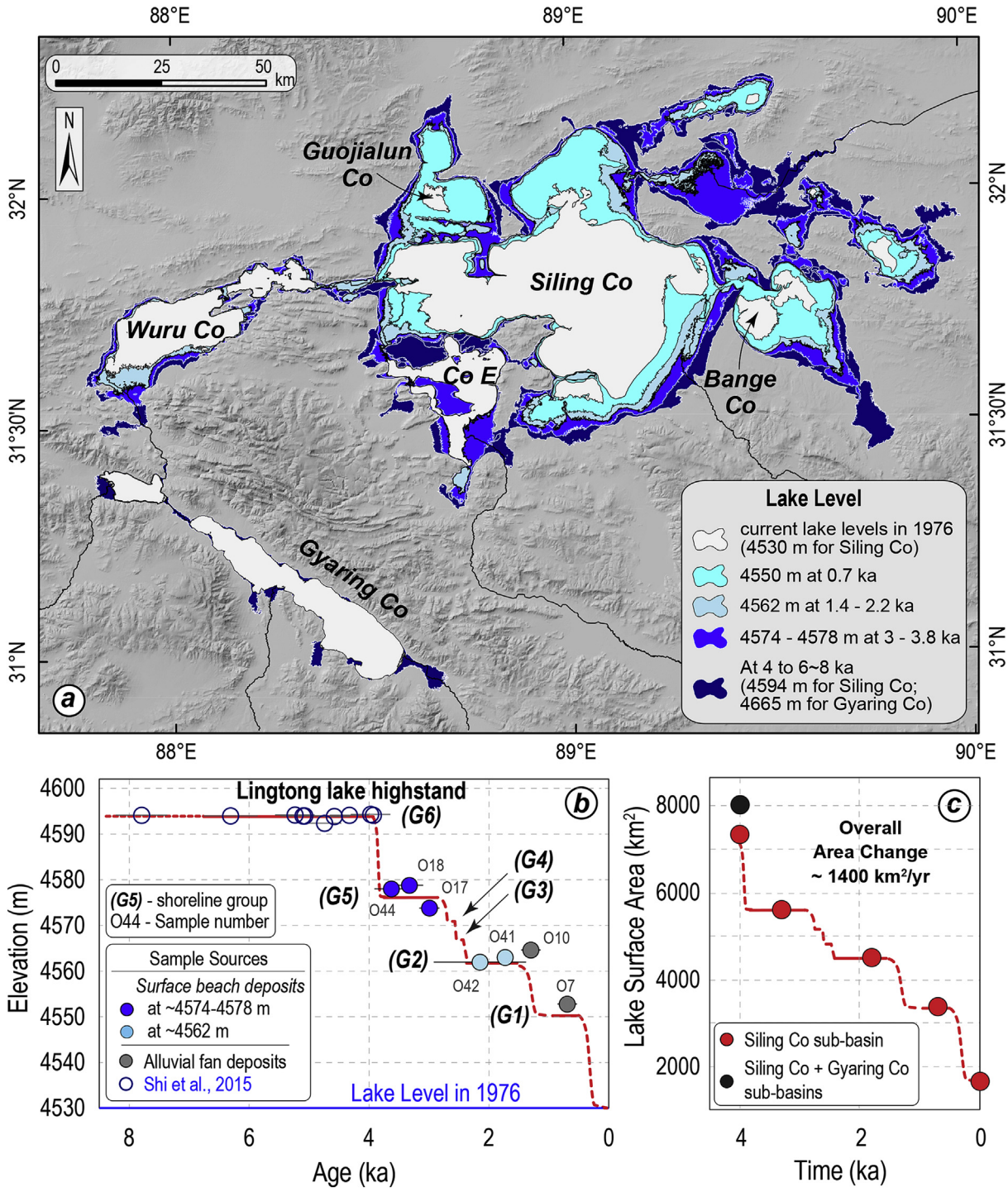

Fig. 9. Reconstructed changes in lake level and surface area of Siling Co and Gyaring Co during the Holocene. (a) Map showing lake surface area of the Siling Co and Gyaring Co at 4 stillstands (corresponding to groups G6, G5, G2, and G1). Map was determined by taking surveyed elevations and determining their position from the 90-m-resolution Shuttle Radar Topographic Mission (SRTM) topographic data. The lake area of Siling Co in 1976 has been provided in Meng et al. (2012a), and elevation of the highstand level at Gyaring Co is from Shi et al. (2014). (b) Shoreline elevations vs. corresponding OSL ages from highstand and recessional deposits. Color code of the circles are the same as those in Fig. 9a. (c) Change in lake surface area through time. The black dot shows the contribution of lake area change from Gyaring Co. The red line shows the possible area change path, inferred from the lake level change on the left. (For interpretation of the references to colour in this figure legend, the reader is referred to the web version of this article.)

7. Discussion

7.1. Delayed onset of recession at Siling Co

The combined dating of recessional shorelines presented here and the results of Shi et al. (2015) (Fig. 10a) are consistent with estimates of relative lake expansion and contraction (Gu et al., 1993; Kashiwaya et al., 1995) inferred from $\delta^{18}O$ variations in a shallow lacustrine core (Fig. 10b). Both datasets demonstrate that the lake remained high during the interval from ~8 to 4 ka, but that the system became strongly evaporative around 4 ka and lake level dropped quickly. The consistency of the two records provides

Table 1
OSL sample data for recessional shorelines below the Lingtong lake highstand.

Shoreline group	Sample name	Lat (°N)	Long (°E)	Samp elev (m)	Depth (m)	N[a]	Dose rate (Gy/ka)	Error (Gy/ka)	De (Gy)	Error (Gy)	Age (Ka)	Error (Ka)	Age model[b]	Position[c]
G5	O18	31.64	88.894	4578.1	0.7	51	2.85	0.11	9.47	0.53	3.3	0.2	MAM-3	B
	O17	31.64	88.895	4572.3	1.5	59	3.56	0.07	10.67	0.55	3	0.2	MAM-3	B
	O44	31.653	88.91	4576.5	1.5	51	1.7	0.05	6.18	0.44	3.6	0.3	MAM-3	B
G2	O10	31.654	88.914	4564.2	0.4	50	3.26	0.14	4.24	0.5	1.3	0.2	MAM-3	A
	O41	31.654	88.914	4563	1.8	51	3.18	0.06	5.51	0.43	1.7	0.1	MAM-3	B
	O42	31.654	88.914	4561.2	0.8	54	1.9	0.05	4.09	1.46	2.2	0.8	MAM-3	B
G1	O7	31.659	88.916	4552.4	0.4	53	4.03	0.07	2.8	0.1	0.7	0	CAM	A

[a] N is the number of aliquots used for OSL analysis.
[b] CAM – central age model; MAM – minimum age model; numbers denote the component of each age model.
[c] Position denotes the depositional environment of the samples. A – samples in the alluvial sediments; B – samples in the top layers of the beach ridges.

confidence that our inferences of both the timing and magnitude of changes in lake size and lake level at Siling Co are robust. The isotope data (Gu et al., 1993; Kashiwaya et al., 1995) provide an additional constraint that the lake rose and expanded to reach its highstand condition from ~10.5–9.5 ka from a previously lower level (Fig. 10a and b). The lake then remained high between ~9.5–4 ka, and receded in a stepwise manner during the late Holocene (Fig. 10b).

The history of Siling Co differs notably from that of other Tibetan lakes, in particular with regard to the timing of when recession began. Several lakes in western Tibet began to recede near to the Late Pleistocene-Holocene transition, between 11 and 8 ka (Chen et al., 2013; Hudson et al., 2015; Liu et al., 2016; Rades et al., 2015) (Fig. 10c). Moreover, the onset of this recession may have migrated from west to east across the Tibetan Plateau (Hudson and Quade, 2013). In contrast, Siling Co appears to have remained at its maximum Late Pleistocene-Holocene extent until ~4 ka.

Despite the differences in the onset time of lake recessions between Siling Co and other Tibetan lakes, the tempo of recession of several other lakes (Hudson and Quade, 2013; Hudson et al., 2015) (Fig. 10a and d) appears to have been punctuated with short-lived stillstands. In this context, the interpretation of monotonic recession of Zhari Namco (Chen et al., 2013) and Tangra Yumco (Rades et al., 2015) (Fig. 10c) may simply be a consequence of the relatively sparse datasets in these studies. In fact, recent new dates of shoreline deposits around Tangra Yumco (Ahlborn et al., 2016) and the 'outlier' data in Rades et al. (2015) (open circles in Fig. 10c) suggest to us that the recession of Tangra Yumco was also likely punctuated by stillstands during the latter half of the Holocene (the green dashed line in Fig. 10c).

7.2. Constraints on the strength of the Asian monsoon

Our determination of the lake surface area changes and the *HI* allow us to place some semi-quantitative bounds on changes of the effective moisture over Siling Co region. The *HI* appears to have been three times greater at the onset of recession at ~4 ka than it is today (Table S3). These results together with the stepwise lake recession process (Fig. 10a) reflect a general decrease in the effective moisture in the Siling Co region during the Late Holocene. These observations are consistent with previous suggestions of a general cooling and drying trend since 6–4 ka based on temperature proxy of $\delta^{18}O$ from the Guliya ice core in central Tibet (Thompson et al., 1997) and pollen records of central Tibetan lakes (Herzschuh et al., 2006; Li et al., 2011; Mügler et al., 2010; Shen et al., 2008) (Fig. 10f–h), of other lake core proxies (Bird et al., 2014; Gasse et al., 1991, 1996) (Fig. 10d–e), and from a synthesis of paleo-effective moisture across much of Tibet (Herzschuh, 2006). Since only one minor glacial advance has been described from central Tibet during this time, at ~2.8 ka (Yi et al., 2008), we believe it is likely that changes in lake level were most likely driven by changes in precipitation associated with the monsoon. The approximate 3-fold change in the *HI* index of Siling Co is also generally consistent with the qualitative estimates of paleo-precipitation changes inferred from stalagmite $\delta^{18}O$ records (Fig. 11c–d) in central Tibet (Cai et al., 2012) and east China (Wang et al., 2005).

7.3. Variable response of Siling Co to abrupt Holocene climate change

Paleoclimate archives from marine and terrestrial deposits indicate that the monsoon was significantly weaker than present during the last glacial period (ca. 20–18 ka), strengthened in the early Holocene, and decreased to the present (An et al., 2015; Overpeck et al., 1996). Climate simulations suggest that these millennial-scale variations reflect two fundamental drivers: 1) changing solar insolation due to variations in the Earth's orbit (Fig. 11e) that influence the degree of warming of the Asian landmass (Kutzbach, 1981; Prell, 1984; Prell and Kutzbach, 1992), and 2) variations in ice volume, sea surface temperature, and heat transport by atmosphere/ocean circulation associated with changes in glacial-interglacial boundary conditions (Manabe and Broccoli, 1985; Overpeck et al., 1989, 2006; Prell and Kutzbach, 1987; Wang et al., 2005). Although solar insolation appears to be the primary driver of millennial-scale variations (Clemens et al., 1991; Clemens and Prell, 1991), feedbacks associated with glacial-interglacial changes appear to be responsible for abrupt strengthening/weakening of the monsoon in latest Pleistocene time (Altabet et al., 2002; Henry et al., 2016; Overpeck et al., 1996; Schulz et al., 1998; Wang et al., 2001).

Recently, however, proxy data imply that changes in monsoon strength also occurred during the Holocene (Gasse and Van Campo, 1994; Street-Perrott and Perrott, 1990); these appear to correlate with subtle but persistent cyclicity in north Atlantic sedimentologic records (e.g., the ice-rafted debris records, Fig. 11i, Bond et al., 2001). The intensity of upwelling in the Arabian Sea (e.g., Fig. 11f), a direct proxy for the strength of monsoon winds (Anderson and Prell, 1993; Prell et al., 1990), suggests a correlation between periods of weakened monsoon circulation and cold periods in the North Atlantic (Gupta et al., 2003). Similarly, variations in the intensity of monsoonal precipitation over the Asian continent are inferred from shifts in the stable isotopic (e.g., $\delta^{18}O$) composition of speleothem carbonate (Fig. 11c–d) (e.g., Cai et al., 2012; Dykoski et al., 2005; Fleitmann et al., 2003; Wang et al., 2005), ice cores (e.g., Thompson et al., 2000), and peat bogs (Hong et al., 2003). Notably, studies suggest at least two periods of weak monsoonal circulation, at ~8 ka (Cheng et al., 2009; Dixit

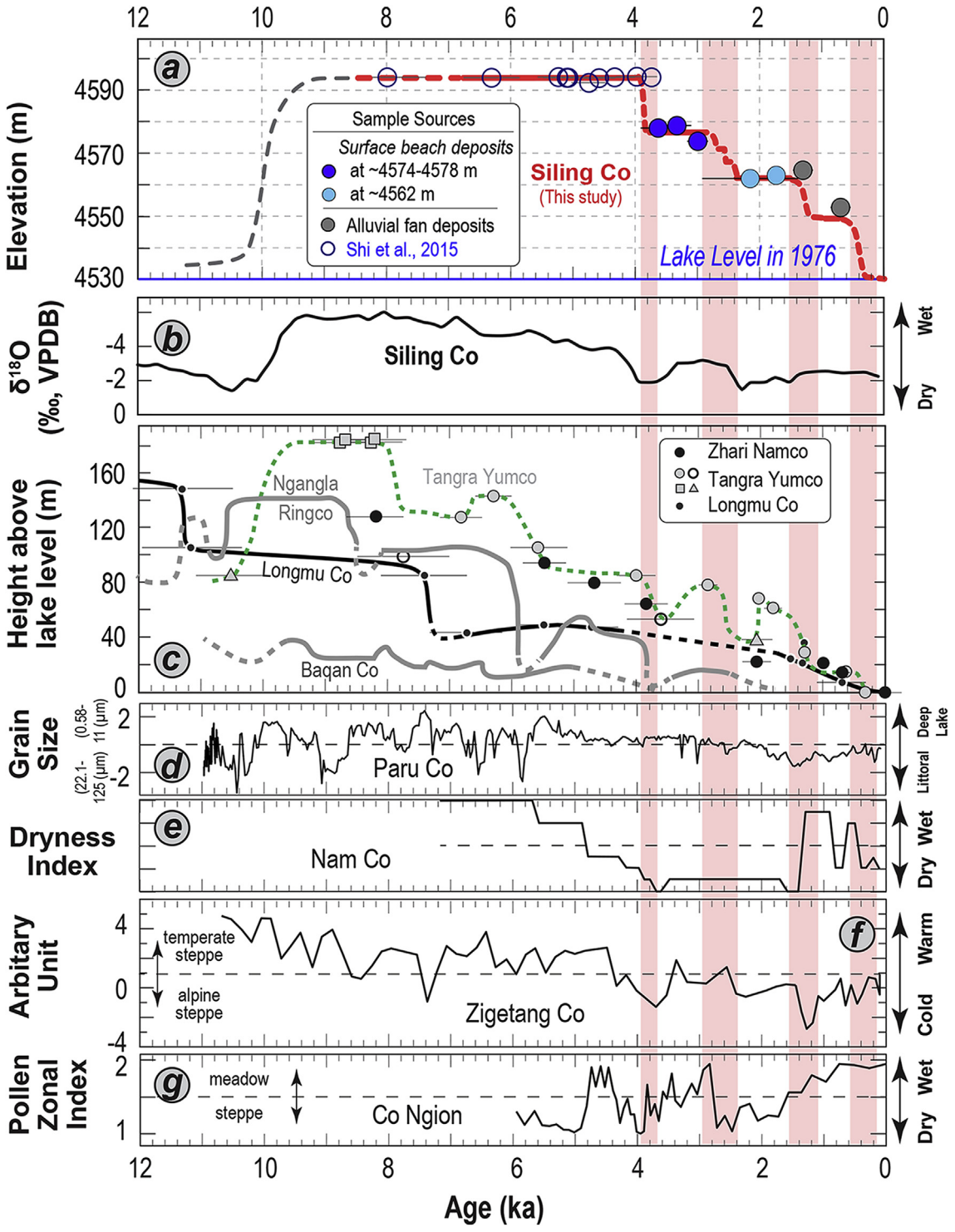

Fig. 10. Comparison of the lake level change of Siling Co with other lake level curves and lake core proxies from the Tibetan Plateau. (a) Lake level changes of Siling Co (also see details in the captions of Fig. 9b). The circles show OSL ages from shoreline deposits, with the same color codes as Fig. 9b. The thick red lines are lake level change suggested by our data; solid and dashed red lines show well-determined and inferred lake levels, respectively. The gray dashed line shows the lake history inferred from the carbonate $\delta^{18}O$ record of Siling Co (see Fig. 10b). The light pink bars show approximate time periods of rapid lake recession. (b) Carbonate $\delta^{18}O$ records of Siling Co (Gu et al., 1993). (c) Shoreline-derived lake level changes for lakes in western Tibet: Longmu Co (Liu et al., 2016), Ngangla Ring Co (Hudson et al., 2015), Baqan Co (Huth et al., 2015), Zhari Namco (Chen et al., 2013). The green dashed line represents our interpretation of possible stepwise recession of Tangra Yumco based on newly published shoreline data (Ahlborn et al., 2016) and the 'outlier' data in previous studies (Rades et al., 2013, 2015). (d) Grain size index of Paru Co suggesting changes in lake depth through time (Bird et al., 2014). (e–g) Pollen records from Nam Co (Mügler et al., 2010), Zigetang Co (Herzschuh et al., 2006) and Co Ngion (Shen et al., 2008), respectively. (For interpretation of the references to colour in this figure legend, the reader is referred to the web version of this article.)

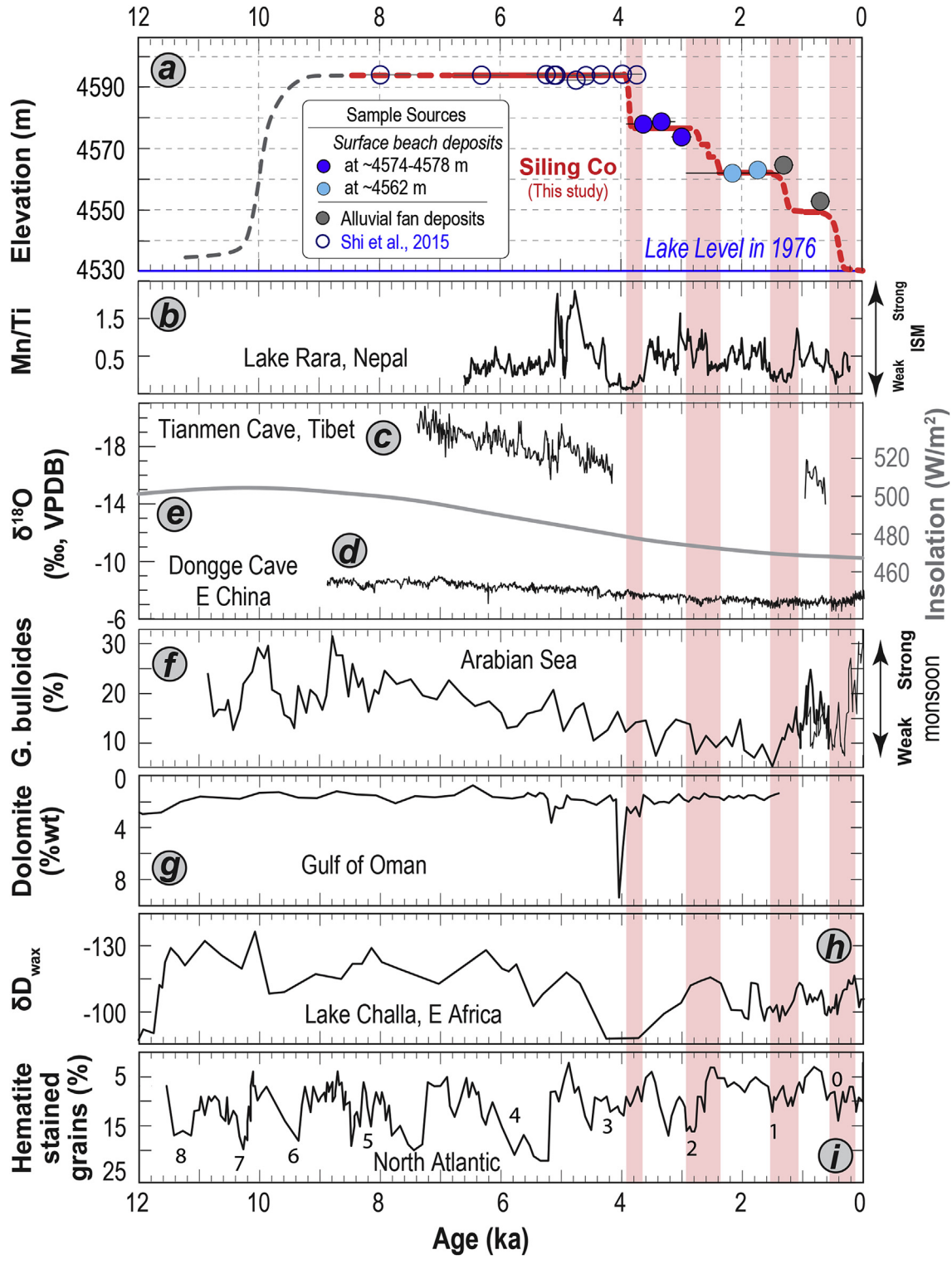

Fig. 11. Comparison of lake level changes of Siling Co with paleoclimatic proxies suggesting changes in the strength of the Asian monsoon. (a) Lake level changes at Siling Co, same as shown in Fig. 8a. (b) Mn/Ti ratios from Lake Rara, Nepalese Himalaya (Nakamura et al., 2016). (c–d) $\delta^{18}O$ records from speleothems in Tianmen Cave in central Tibet (Cai et al., 2012) (see location in Fig. 1) and Dongge Cave (Wang et al., 2005) in east China, respectively. (e) Insolation change at 30°N (Berger, 1978). (f) Upwelling record (relative abundance of G. bulloides) from the Arabian Sea (Gupta et al., 2003). (g) Changes in dolomite concentration in the Gulf of Oman (Cullen et al., 2000). (h) δD_{wax} record from biomarkers in Lake Challa, east Africa (Tierney et al., 2011). (i) Changes of percentage of hematite-stained grains in the North Atlantic (Bond et al., 2001).

et al., 2014b; Gupta et al., 2003) and ~4 ka (Dixit et al., 2014a; Nakamura et al., 2016; Prasad et al., 2014). These time periods are characterized by severe aridity in both Africa and Asia, and the younger of these two events has been suggested to have precipitated the cultural collapse of early societies in Asia (Berkelhammer et al., 2012; Cullen et al., 2000).

Comparison of our reconstruction of lake levels at Siling Co with regional datasets (Fig. 10a) suggests that lake systems in Tibet may

have experienced a spatially variable response to the climate shifts at ~8 ka (Dixit et al., 2014b; Gupta et al., 2003; Zhu et al., 2015) and ~4 ka (Cullen et al., 2000; Nakamura et al., 2016). Whereas highstand conditions at Siling Co appear to have been maintained throughout the 8-ka event (Fig. 10a), initial recession of the lake is coincident with the abrupt drying and cooling observed around ~4 ka (Fig. 10a) both within the Tibetan region (Fig. 10d and f–h) and in other regions (e.g., East China, Nepalese Himalaya, Arabian Sea and East Africa) influenced by the Asian monsoon (Fig. 11b–i). Subsequent rapid lake recessions of Siling Co after 4 ka (Fig. 10a) appear to broadly correlate with the cold/dry events found elsewhere within Tibet (Fig. 10), and we believe it is reasonable to suggest that the rapid recessions reflect centennial-scale shifts in climate during the Late Holocene (e.g., Bond et al., 2001; Gupta et al., 2003).

Although the drivers for the differences in the response of Siling Co to abrupt climate events at ~8 ka and ~4 ka, remain uncertain, the response of lakes in western Tibet, Ngangla Ringco and Tangra Yumco, may offer some insight. Both of these lakes appear to have receded rapidly in response to both the ~8 ka and ~4 ka events (Fig. 10). Both lakes exist in much smaller watersheds than that of Siling Co, and both lie to the west of Siling Co. It is possible that the size of the Siling Co basin buffered the system response to short-lived climate shifts, but it also seems likely that an eastward gradient of decreasing monsoon precipitation during the early Holocene (Hudson and Quade, 2013), may have driven a greater reduction in precipitation in western lakes at or around ~8 ka. In addition, the Siling Co basin contains numerous valley glaciers and a regional ice cap in the Tanggula Shan, along the northern part of the watershed (Fig. 2) (Owen and Dortch, 2014; Yi et al., 2008). Although glacial melting appears to have a secondary effect on historic lake level change (Tong et al., 2016; Zhou et al., 2015), glacial meltwater delivery to Siling Co may have been a contribution to highstand conditions in the early Holocene. Higher temperatures during this time are suggested from pollen records (Herzschuh et al., 2006; Li et al., 2011; Mügler et al., 2010; Shen et al., 2008; Van Campo et al., 1996), and increased meltwater from the Tanggula Shan may have offset reduced monsoon precipitation at ~8 ka. A test of this hypothesis awaits a more refined chronology of the glacial history in the Tanggula Shan.

8. Conclusions

Mapping, surveying and OSL dating of a sequence of recessional shorelines and associated alluvial fan features around Siling Co, in central Tibet, place constraints on lake level history during the Holocene. Our results show that Siling Co experienced rapid and punctuated lake recession since ~4 ka, following a long-lived highstand between ~9 and 4 ka. Determination of lake surface area change and estimation of past hydrologic indices of the Siling Co region suggests the effective moisture during the early Holocene highstand was approximately three times greater than today. These observations provide a semi-quantitative constraint on the general weakening of the Asian monsoon during the Late Holocene. Moreover, Holocene recession of Siling Co appears to differ from other lakes in western and central Tibet that began to recede in the Early Holocene. The contrasting response of Siling Co to two abrupt changes in climate at ~8 ka and ~4 ka may reflect effects of enhanced glacial melting during the early Holocene. Overall, we conclude that the Holocene lake level history of Siling Co reflects a gradual weakening of the Asian monsoon on centennial to millennial scale, but this was modulated by several periods of more abrupt climate change.

Acknowledgments

This work was supported by a National Science Foundation grant from the Tectonics program (EAR-0911587) to E.K. and K.P.F. Additional support to E.W. was provided by grants from the Chinese Academy of Sciences (XDB03010500). X.S. also thanks the support from the Earth Observatory of Singapore, Nanyang Technological University through its funding from the National Research Foundation Singapore and the Singapore Ministry of Education under the Research Centers of Excellence initiative. This work comprises Earth Observatory of Singapore contribution number 158. We are grateful to Tashi Wangdi and Feng Qu for assistance with the field work. Dr. Xianfeng Wang provided some feedbacks on an early version of the manuscript. We thank Editor Ana Moreno for the editorial handling of this paper, and thank Adam Hudson and one anonymous reviewer for providing constructive comments that helped improve the quality of this paper. We declare no financial interests among the authors. Supporting data can be accessed in the Supporting Material file.

Appendix A. Supplementary data

Supplementary data related to this article can be found at http://dx.doi.org/10.1016/j.quascirev.2017.07.017.

References

Adamiec, G., Aitken, M., 1998. Dose-rate conversion factors: update. Anc. tL 16, 37–50.
Ahlborn, M., Haberzettl, T., Wang, J., Fürstenberg, S., Mäusbacher, R., Mazzocco, J., Pierson, J., Zhu, L., Frenzel, P., 2016. Holocene lake level history of the Tangra Yumco lake system, southern-central Tibetan Plateau. Holocene 26, 176–187.
Aitken, M.J., 1998. An Introduction to Optical Dating: the Dating of Quaternary Sediments by the Use of Photon-stimulated Luminescence. Oxford University Press.
Altabet, M.A., Higginson, M.J., Murray, D.W., 2002. The effect of millennial-scale changes in Arabian Sea denitrification on atmospheric CO2. Nature 415, 159–162.
An, Z., Wu, Jianping, L., Youbin, S., Yimin, L., Weijian, Z., Cai, Y., Duan, A., Li, L., Mao, J., Cheng, H., Shi, Z., Tan, L., Yan, H., Ao, H., Chang, H., Feng, J., 2015. Global monsoon dynamics and climate change. Annu. Rev. Earth Planet. Sci. 43, 29–77.
Anderson, D.M., Prell, W.L., 1993. A 300 KYR record of upwelling off Oman during the late quaternary: evidence of the Asian Southwest monsoon. Paleoceanography 8, 193–208.
Arnold, L.J., Roberts, R.G., 2009. Stochastic modelling of multi-grain equivalent dose (De) distributions: implications for OSL dating of sediment mixtures. Quat. Geochronol. 4, 204–230.
Banerjee, D., Bøtter-Jensen, L., Murray, A., 2000. Retrospective dosimetry: estimation of the dose to quartz using the single-aliquot regenerative-dose protocol. Appl. Radiat. Isotopes 52, 831–844.
Benson, L.V., Currey, D.R., Dorn, R.I., Lajoie, K.R., Oviatt, C.G., Robinson, S.W., Smith, G.I., Stine, S., 1990. Chronology of expansion and contraction of four Great Basin lake systems during the past 35,000 years. Palaeogeogr. Palaeoclimatol. Palaeoecol. 78, 241–286.
Benson, L.V., Paillet, F.L., 1989. The use of total lake-surface area as an indicator of climatic change: examples from the Lahontan basin. Quat. Res. 32, 262–275.
Berger, A., 1978. Long-term variations of caloric insolation resulting from the earth's orbital elements. Quat. Res. 9, 139–167.
Berkelhammer, M., Sinha, A., Stott, L., Cheng, H., Pausata, F., Yoshimura, K., 2012. An abrupt shift in the Indian monsoon 4000 years ago. Clim. landscapes, civilizations 75–88.
Bird, B.W., Polisar, P.J., Lei, Y., Thompson, L.G., Yao, T., Finney, B.P., Bain, D.J., Pompeani, D.P., Steinman, B.A., 2014. A Tibetan lake sediment record of Holocene Indian summer monsoon variability. Earth Planet. Sci. Lett. 399, 92–102.
Bond, G., Kromer, B., Beer, J., Muscheler, R., Evans, M.N., Showers, W., Hoffmann, S., Lotti-Bond, R., Hajdas, I., Bonani, G., 2001. Persistent solar influence on North Atlantic climate during the Holocene. Science 294, 2130–2136.
Cai, Y., Zhang, H., Cheng, H., An, Z., Lawrence Edwards, R., Wang, X., Tan, L., Liang, F., Wang, J., Kelly, M., 2012. The Holocene Indian monsoon variability over the southern Tibetan Plateau and its teleconnections. Earth Planet. Sci. Lett. 335–336, 135–144.
Chen, Y., Zong, Y., Li, B., Li, S., Aitchison, J.C., 2013. Shrinking lakes in Tibet linked to the weakening Asian monsoon in the past 8.2 ka. Quat. Res. 80, 189–198.
Cheng, H., Fleitmann, D., Edwards, R.L., Wang, X., Cruz, F.W., Auler, A.S., Mangini, A., Wang, Y., Kong, X., Burns, S.J., 2009. Timing and structure of the 8.2 kyr BP event inferred from $\delta^{18}O$ records of stalagmites from China, Oman, and Brazil. Geology 37, 1007–1010.
Clemens, S., Prell, W., Murray, D., Shimmield, G., Weedon, G., 1991. Forcing mechanisms of the indian ocean monsoon. Nature 353, 720–725.
Clemens, S.C., Prell, W.L., 1991. Late Quaternary forcing of Indian Ocean summer-

monsoon winds: a comparison of Fourier model and general circulation model results. J. Geophys. Res. Atmos. 96, 22683–22700.
Cullen, H.M., Hemming, S., Hemming, G., Brown, F., Guilderson, T., Sirocko, F., 2000. Climate change and the collapse of the Akkadian empire: evidence from the deep sea. Geology 28, 379–382.
Dayem, K.E., Molnar, P., Battisti, D.S., Roe, G.H., 2010. Lessons learned from oxygen isotopes in modern precipitation applied to interpretation of speleothem records of paleoclimate from eastern Asia. Earth Planet. Sci. Lett. 295, 219–230.
Dixit, Y., Hodell, D.A., Petrie, C.A., 2014a. Abrupt weakening of the summer monsoon in northwest India ~4100 yr ago. Geology 42, 339–342.
Dixit, Y., Hodell, D.A., Sinha, R., Petrie, C.A., 2014b. Abrupt weakening of the Indian summer monsoon at 8.2 kyr B.P. Earth Planet. Sci. Lett. 391, 16–23.
Doin, M.-P., Twardzik, C., Ducret, G., Lasserre, C., Guillaso, S., Jianbao, S., 2015. InSAR measurement of the deformation around Siling Co Lake: inferences on the lower crust viscosity in central Tibet. J. Geophys. Res. Solid Earth 120, 2014JB011768.
Dykoski, C., Edwards, R., Cheng, H., Yuan, D., Cai, Y., Zhang, M., Lin, Y., Qing, J., An, Z., Revenaugh, J., 2005. A high-resolution, absolute-dated Holocene and deglacial Asian monsoon record from Dongge Cave, China. Earth Planet. Sci. Lett. 233, 71–86.
Farr, T.G., Rosen, P.A., Caro, E., Crippen, R., Duren, R., Hensley, S., Kobrick, M., Paller, M., Rodriguez, E., Roth, L., Seal, D., Shaffer, S., Shimada, J., Umland, J., Werner, M., Oskin, M., Burbank, D., Alsdorf, D., 2007. The shuttle radar topography mission. Rev. Geophys. 45, RG2004.
Fleitmann, D., Burns, S.J., Mudelsee, M., Neff, U., Kramers, J., Mangini, A., Matter, A., 2003. Holocene forcing of the indian monsoon recorded in a stalagmite from Southern Oman. Science 300, 1737–1739.
Galbraith, R., Green, P., 1990. Estimating the component ages in a finite mixture. Int. J. Radiat. Appl. Instrum. Part D. Nucl. Tracks Radiat. Meas. 17, 197–206.
Galbraith, R.F., Roberts, R.G., 2012. Statistical aspects of equivalent dose and error calculation and display in OSL dating: an overview and some recommendations. Quat. Geochronol. 11, 1–27.
Galbraith, R.F., Roberts, R.G., Laslett, G.M., Yoshida, H., Olley, J.M., 1999. Optical dating of single and multiple grains of quartz from jinmium rock shelter, northern australia: part i, experimental design and statistical models*. Archaeometry 41, 339–364.
Gasse, F., Arnold, M., Fontes, J.C., Fort, M., Gibert, E., Huc, A., Bingyan, L., Yuanfang, L., Qing, L., Melieres, F., Campo, E.V., Fubao, W., Qingsong, Z., 1991. A 13,000-year climate record from western Tibet. Nature 353, 742–745.
Gasse, F., Fontes, J.C., Van Campo, E., Wei, K., 1996. Holocene environmental changes in bangong Co basin (Western Tibet). Part 4: discussion and conclusions. Palaeogeogr. Palaeoclimatol. Palaeoecol. 120, 79–92.
Gasse, F., Van Campo, E., 1994. Abrupt post-glacial climate events in West Asia and North Africa monsoon domains. Earth Planet. Sci. Lett. 126, 435–456.
Gu, Z., Liu, J., Yuan, B., Liu, R., Liu, Y., Yaskawa, K., 1993. Monsoon variations of the Qinghai-Xizang plateau during the last 12000 Years-Geochemical evidence from the sediments in the Siling lake. Chin. Sci. Bull. 38, 577–581.
Gupta, A.K., Anderson, D.M., Overpeck, J.T., 2003. Abrupt changes in the Asian southwest monsoon during the Holocene and their links to the North Atlantic ocean. Nature 421, 354–356.
Henry, L.G., McManus, J.F., Curry, W.B., Roberts, N.L., Piotrowski, A.M., Keigwin, L.D., 2016. North Atlantic ocean circulation and abrupt climate change during the last glaciation. Science 353, 470–474.
Herzschuh, U., 2006. Palaeo-moisture evolution in monsoonal Central Asia during the last 50,000 years. Quat. Sci. Rev. 25, 163–178.
Herzschuh, U., Winter, K., Wunnemann, B., Li, S., 2006. A general cooling trend on the central Tibetan Plateau throughout the Holocene recorded by the Lake Zigetang pollen spectra. Quat. Int. 154–155, 113–121.
Hong, Y.T., Hong, B., Lin, Q.H., Zhu, Y.X., Shibata, Y., Hirota, M., Uchida, M., Leng, X.T., Jiang, H.B., Xu, H., Wang, H., Yi, L., 2003. Correlation between indian ocean summer monsoon and North Atlantic climate during the Holocene. Earth Planet. Sci. Lett. 211, 371–380.
Hudson, A.M., Quade, J., 2013. Long-term east-west asymmetry in monsoon rainfall on the Tibetan Plateau. Geology 41, 351–354.
Hudson, A.M., Quade, J., Huth, T.E., Lei, G., Cheng, H., Edwards, L.R., Olsen, J.W., Zhang, H., 2015. Lake level reconstruction for 12.8–2.3 ka of the Ngangla Ring Tso closed-basin lake system, southwest Tibetan Plateau. Quat. Res. 83, 66–79.
Huth, T., Hudson, A.M., Quade, J., Guoliang, L., Hucai, Z., 2015. Constraints on paleoclimate from 11.5 to 5.0 ka from shoreline dating and hydrologic budget modeling of Baqan Tso, southwestern Tibetan Plateau. Quat. Res. 83, 80–93.
Kashiwaya, K., Masuzawa, T., Morinaga, H., Yaskawa, K., Baoyin, Y., Jiaqi, L., Zhaoyan, G., 1995. Changes in hydrological conditions in the central Qing-Zang (Tibetan) Plateau inferred from lake bottom sediments. Earth Planet. Sci. Lett. 135, 31–39.
Kong, P., Na, C.G., Fink, D., Huang, F.X., Ding, L., 2007. Cosmogenic Be-10 inferred lake-level changes in Sumxi Co basin, Western Tibet. J. Asian Earth Sci. 29, 698–703.
Kreutzer, S., Schmidt, C., Fuchs, M.C., Dietze, M., Fischer, M., Fuchs, M., 2012. Introducing an R package for luminescence dating analysis. Anc. TL 30, 1–8.
Kutzbach, J.E., 1981. Monsoon climate of the early Holocene: climate experiment with the earth's orbital parameters for 9000 years ago. Science 214, 59–61.
Li, Q., Lu, H., Zhu, L., Wu, N., Wang, J., Lu, X., 2011. Pollen-inferred climate changes and vertical shifts of alpine vegetation belts on the northern slope of the Nyainqentanglha Mountains (central Tibetan Plateau) since 8.4 kyr BP. Holocene, 0959683611400218.
Liu, X.-J., Madsen, D.B., Liu, R., Sun, Y., Wang, Y., 2016. Holocene lake level variations of Longmu Co, western Qinghai-Tibetan Plateau. Environ. Earth Sci. 75, 1–14.
Manabe, S., Broccoli, A., 1985. The influence of continental ice sheets on the climate of an ice age. J. Geophys. Res. 90, 2167–2190.
Mejdahl, V., 1979. Thermoluminescence dating: beta-dose attenuation in quartz grains. Archaeometry 21, 61–72.
Meng, K., Shi, X., Wang, E., Liu, F., 2012a. High-altitude salt lake elevation changes and glacial ablation in Central Tibet, 2000–2010. Chin. Sci. Bull. 57, 525–534.
Meng, K., Shi, X., Wang, E., Su, Z., 2012b. Geomorphic characteristics, spatial distribution of paleoshorelines around the Siling Co area, central Tibet, and the lake evolution within the plateau. Chin. J. Geol. 47, 730–745 (in Chinese with English abstract).
Mifflin, M.D., Wheat, M.M., 1979. Pluvial Lakes and Estimated Pluvial Climates of Nevada. Mackay School of Mines, University of Nevada.
Mischke, S., Zhang, C., 2010. Holocene cold events on the Tibetan plateau. Glob. Planet. Change 72, 155–163.
Morrill, C., Overpeck, J.T., Cole, J.E., Liu, K.-b., Shen, C., Tang, L., 2006. Holocene variations in the Asian monsoon inferred from the geochemistry of lake sediments in central Tibet. Quat. Res. 65, 232–243.
Mügler, I., Gleixner, G., Günther, F., Mäusbacher, R., Daut, G., Schütt, B., Berking, J., Schwalb, A., Schwark, L., Xu, B., Yao, T., Zhu, L., Yi, C., 2010. A multi-proxy approach to reconstruct hydrological changes and Holocene climate development of Nam Co, Central Tibet. J. Paleolimnol. 43, 625–648.
Murray, A.S., Wintle, A.G., 2000. Luminescence dating of quartz using an improved single-aliquot regenerative-dose protocol. Radiat. Meas. 32, 57–73.
Nakamura, A., Yokoyama, Y., Maemoku, H., Yagi, H., Okamura, M., Matsuoka, H., Miyake, N., Osada, T., Adhikari, D.P., Dangol, V., Ikehara, M., Miyairi, Y., Matsuzaki, H., 2016. Weak monsoon event at 4.2 ka recorded in sediment from Lake Rara, Himalayas. Quat. Int. 397, 349–359.
Overpeck, J., Anderson, D., Trumbore, S., Prell, W., 1996. The southwest Indian Monsoon over the last 18 000 years. Clim. Dyn. 12, 213–225.
Overpeck, J., Peterson, L.C., Kipp, N., Imbrie, J., Rind, D., 1989. Climate change in the circum-North Atlantic region during the last deglaciation. Nature 338, 553–557.
Overpeck, J.T., Otto-Bliesner, B.L., Miller, G.H., Muhs, D.R., Alley, R.B., Kiehl, J.T., 2006. Paleoclimatic evidence for future ice-sheet instability and rapid sea-level rise. Science 311, 1747–1750.
Owen, L.A., Dortch, J.M., 2014. Nature and timing of quaternary glaciation in the himalayan–Tibetan orogen. Quat. Sci. Rev. 88, 14–54.
Prasad, S., Anoop, A., Riedel, N., Sarkar, S., Menzel, P., Basavaiah, N., Krishnan, R., Fuller, D., Plessen, B., Gaye, B., 2014. Prolonged monsoon droughts and links to Indo-Pacific warm pool: a Holocene record from Lonar Lake, central India. Earth Planet. Sci. Lett. 391, 171–182.
Prell, W.L., 1984. Variation of monsoonal upwelling: a response to changing solar radiation. Clim. Process. Clim. Sensit. 48–57.
Prell, W.L., Kutzbach, J.E., 1987. Monsoon variability over the past 150,000 years. J. Geophys. Res. Atmos. 92, 8411–8425.
Prell, W.L., Kutzbach, J.E., 1992. Sensitivity of the Indian monsoon to forcing parameters and implications for its evolution. Nature 360, 647–652.
Prell, W.L., Marvil, R.E., Luther, M.E., 1990. Variability in upwelling fields in the northwestern Indian Ocean 2. Data-model comparison at 9000 years BP. Paleoceanography 5, 447–457.
Prescott, J., Hutton, J.T., 1994. Cosmic ray contributions to dose rates for luminescence and ESR dating: large depths and long-term time variations. Radiat. Meas. 23, 497–500.
Rades, E.F., Hetzel, R., Xu, Q., Ding, L., 2013. Constraining Holocene lake-level highstands on the Tibetan Plateau by 10Be exposure dating: a case study at Tangra Yumco, southern Tibet. Quat. Sci. Rev. 82, 68–77.
Rades, E.F., Tsukamoto, S., Frechen, M., Xu, Q., Ding, L., 2015. A lake-level chronology based on feldspar luminescence dating of beach ridges at Tangra Yum Co (southern Tibet). Quat. Res. 83, 469–478.
Readhead, M., 2002a. Absorbed dose fraction for 87Rb β particles. Anc. TL 20, 25–27.
Readhead, M., 2002b. Addendum to “Absorbed dose fraction for 87Rb β particles”. Anc. TL 20, 47.
Reheis, M.C., Adams, K.D., Oviatt, C.G., Bacon, S.N., 2014. Pluvial lakes in the Great Basin of the western United States—a view from the outcrop. Quat. Sci. Rev. 97, 33–57.
Schulz, H., von Rad, U., Erlenkeuser, H., 1998. Correlation between Arabian Sea and Greenland climate oscillations of the past 110,000 years. Nature 393, 54–57.
Shen, C., Liu, K.-B., Morrill, C., Overpeck, J.T., Peng, J., Tang, L., 2008. Ecotone shift and major droughts during the mid-late Holocene in the central Tibetan Plateau. Ecology 89, 1079–1088.
Shi, X., Furlong, K.P., Kirby, E., Meng, K., Marrero, S., Gosse, J., Wang, E., Phillips, F., 2017. Evaluating the size and extent of paleolakes in central Tibet during the late Pleistocene. Geophys. Res. Lett. 44, 5476–5485.
Shi, X., Kirby, E., Furlong, K.P., Meng, K., Robinson, R., Wang, E., 2015. Crustal strength in central Tibet determined from Holocene shoreline deflection around Siling Co. Earth Planet. Sci. Lett. 423, 145–154.
Shi, X., Kirby, E., Lu, H., Robinson, R., Furlong, K.P., Wang, E., 2014. Holocene slip rate along the Gyaring Co fault, central Tibet. Geophys. Res. Lett. 41, 2014GL060782.
Street-Perrott, F.A., Perrott, R.A., 1990. Abrupt climate fluctuations in the tropics: the influence of Atlantic Ocean circulation. Nature 343, 607–612.
Sutton, S., Zimmerman, D., 1978. Thermoluminescence dating: radioactivity in quartz. Archaeometry 20, 67–69.
Thompson, L.G., Yao, T., Davis, M.E., Henderson, K.A., Mosley-Thompson, E., Lin, P.-

N., Beer, J., Synal, H.-A., Cole-Dai, J., Bolzan, J.F., 1997. Tropical climate instability: the last glacial cycle from a qinghai-Tibetan ice core. Science 276, 1821–1825.
Thompson, L.G., Yao, T., Mosley-Thompson, E., Davis, M.E., Henderson, K.A., Lin, P.-N., 2000. A high-resolution millennial record of the South Asian monsoon from himalayan ice cores. Science 289, 1916–1919.
Tian, L., Masson-Delmotte, V., Stievenard, M., Yao, T., Jouzel, J., 2001a. Tibetan Plateau summer monsoon northward extent revealed by measurements of water stable isotopes. J. Geophys. Res. Atmos. 106, 28081–28088.
Tian, L., Yao, T., Numaguti, A., Sun, W., 2001b. Stable isotope variations in monsoon precipitation on the Tibetan plateau. J. Meteorological Soc. Jpn. 79, 959–966. Ser. II.
Tierney, J.E., Russell, J.M., Damsté, J.S.S., Huang, Y., Verschuren, D., 2011. Late quaternary behavior of the east African monsoon and the importance of the Congo air boundary. Quat. Sci. Rev. 30, 798–807.
Tong, K., Su, F., Xu, B., 2016. Quantifying the contribution of glacier-melt water in the expansion of the largest lake in Tibet. J. Geophys. Res. Atmos. 121, 11158–11173.
Van Campo, E., Cour, P., Sixuan, H., 1996. Holocene environmental changes in Bangong Co basin (Western Tibet). Part 2: the pollen record. Palaeogeogr. Palaeoclimatol. Palaeoecol. 120, 49–63.
Wang, Y., Cheng, H., Edwards, R.L., He, Y., Kong, X., An, Z., Wu, J., Kelly, M.J., Dykoski, C.A., Li, X., 2005. The Holocene Asian monsoon: links to solar changes and North Atlantic climate. Science 308, 854–857.
Wang, Y.J., Cheng, H., Edwards, R.L., An, Z.S., Wu, J.Y., Shen, C.C., Dorale, J.A., 2001. A high-resolution absolute-dated late Pleistocene monsoon record from hulu cave, China. Science 294, 2345–2348.
Yi, C., Chen, H., Yang, J., Liu, B., Fu, P., Liu, K., Li, S., 2008. Review of Holocene glacial chronologies based on radiocarbon dating in Tibet and its surrounding mountains. J. Quat. Sci. 23, 533–543.
Zhang, G., Yao, T., Xie, H., Zhang, K., Zhu, F., 2014. Lakes' state and abundance across the Tibetan plateau. Chin. Sci. Bull. 1–12.
Zhang, Y., Yao, T., Ma, Y., 2011. Climatic changes have led to significant expansion of endorheic lakes in Xizang (Tibet) since 1995. Sci. Cold Arid Regions 3, 463–467.
Zhou, J., Wang, L., Zhang, Y., Guo, Y., Li, X., Liu, W., 2015. Exploring the water storage changes in the largest lake (Selin Co) over the Tibetan Plateau during 2003-2012 from a basin-wide hydrological modeling. Water Resour. Res. 51, 8060–8086.
Zhu, L., Lü, X., Wang, J., Peng, P., Kasper, T., Daut, G., Haberzettl, T., Frenzel, P., Li, Q., Yang, R., 2015. Climate change on the Tibetan Plateau in response to shifting atmospheric circulation since the LGM. Sci. Rep 5, 13318.
Zhu, L., Peng, P., Xie, M., Wang, J., Frenzel, P., Wrozyna, C., Schwalb, A., 2010. Ostracod-based environmental reconstruction over the last 8,400 years of Nam Co Lake on the Tibetan plateau. Hydrobiologia 648, 157–174.